JOURNAL OF MOLECULAR SPECTROSCOPY **190,** 379–396 (1998)
ARTICLE NO. MS987611

Water Vapor Measurements between 590 and 2582 cm^{-1}: Line Positions and Strengths

Robert A. Toth

Jet Propulsion Laboratory, California Institute of Technology, Pasadena, California 91109

Received March 20, 1998

This study involves measurements of $H_2{}^{16}O$, $H_2{}^{17}O$, and $H_2{}^{18}O$ vapor spectra for the region between 590 and 2582 cm^{-1}. The parameters derived from the data include line positions, energy levels, and linestrengths. The study involves high-resolution line-position measurements with samples at room temperature in the (000)–(000), (010)–(010), and (010)–(000) bands. The experimental frequencies were used along with microwave, far-infrared, and hot water emission measurements in an analysis to obtain high-accuracy rotational energy level values in the (000), and (010) vibrational states of $H_2{}^{16}O$ for $J \leq 20$. The experimental linestrengths were fitted by least squares to a model in which the dipole moment was represented as a series expansion containing up to 19 dipole moment matrix elements. The measurements in this work were more extensive than reported in prior studies by this author for the (010)–(000) band.

1. INTRODUCTION

In earlier studies by this author covering $H_2{}^{16}O$ measurements in the (010)–(000) band (*1*), the (020)–(010) band (*2*), and the (100)–(010) and (001)–(010) bands (*3*), certain spectral regions were inaccessible for measurements due to the presence of a small amount of formamine onto the walls of a 6-m multiple transversal absorption cell. The present set of data were recorded in 1995 and 1996 at the same facility and with the same 6-m absorption cell. However, the majority of the unwanted contaminants were removed prior to recording the data with the aid of a diffusion pump and water vapor absorptions can now be observed for the entire region above 590 cm^{-1}.

This study involves high-resolution measurements of line center positions and strengths in the (000)–(000), (010)–(010), and (010)–(000) bands of $H_2{}^{16}O$ and the (000)–(000) and (010)–(000) bands of $H_2{}^{17}O$ and $H_2{}^{18}O$. The $H_2{}^{16}O$ frequency measurements were used to obtain high-accuracy values of rotational energy levels for the (000), and (010) vibrational states for $J \leq 20$. These measurements were used in conjunction with microwave transitions given by Pearson *et al.* (*4*), far-IR measurements reported by Matsushima *et al.* (*5*), laboratory hot water emission spectra between 370 and 930 cm^{-1} obtained by Polyansky *et al.* (*6*) and further studied by Viti *et al.* (*7*), and sunspot hot water spectra analyzed by Polyansky *et al.* (*8, 9*). Also included in the analysis were previous measurements by this author covering transition frequencies of the (010)–(000) band of $H_2{}^{16}O$ (*1*) and the (010)–(000) bands of $H_2{}^{17}O$ and $H_2{}^{18}O$ (*10*).

The line study analysis included new measurements which were used along with previous measurements (*1*) in a fitting procedure which involved 19 expansion coefficients in the dipole moment for *B*-type transitions. In a recent report, Coudert (*11*) used a new theoretical treatment which involved an analysis of a large data set which included measurements of line positions and strengths of the (010)–(000) band given in my earlier paper (*1*). The results of the linestrength study showed good agreement, on the average, with the measured values and his theoretical model did not require a separation of the data into sets which was required in my earlier analysis (*1*). This theory (*11*) appears superior to the one applied in Ref. (*1*), (and used here) especially for fitting linestrength values over several orders of magnitude as was the case for the experimental data set obtained in this study and a somewhat smaller but similar set given in Ref. (*1*) for the (010)–(000) band of $H_2{}^{16}O$.

The main purpose of this study is to report new experimental results and improvements, if necessary, of previous values (*1, 10*) with the analysis of the data being included as reference for future studies.

2. EXPERIMENT AND SPECTRAL ANALYSIS

The spectra analyzed in this study were recorded with a Fourier transform spectrometer (FTS) located at the McMath solar telescope facility at the Kitt Peak National Observatory. The experimental conditions are given in Table 1. The bottom eight entries with total sample pressures ≤4.86 Torr were used in the line-position analysis. The first eight entries were also used in the self-broadened experiment (*12*) and the following entries given with broadening agents (O_2, N_2, and air) were used in the analysis of the $H_2O + N_2$ and H_2O + air linewidth and frequency-shift study which is another report that follows (*13*), and another study involving H_2O broadened by O_2 (*14*).

Table 1 lists the spectral coverage of the $H_2{}^{16}O$ measurements obtained for each run, unapodized spectral resolution,

0022-2852/98 $25.00

TABLE 1
Experimental Conditions of Spectra Used in the $H_2{}^{16}O$ Measurements

range of measurements (cm^{-1})	unapodized spectral resolution (cm^{-1})	path length (m)	sample pressure (Torr)	sample temperature (K)
1100 - 2400	0.0054	0.25	17.2	301
1100 - 2400	0.0054	0.25	23.2	301
1100 - 2400	0.0054	0.25	27.5	301
1100 - 2400	0.0054	0.25	29.0	302
1100 - 2400	0.0054	0.25	24.1	302
1100 - 2400	0.0054	1.75	18.7	302
1100 - 2400	0.0054	1.75	23.9	302
1100 - 2400	0.0054	1.75	28.5	302
1100 - 2400	0.0054	1.50	0.70, 507.5(O_2)	301
1100 - 2400	0.0054	1.50	0.76, 408.0(O_2)	301
1100 - 2400	0.0054	1.50	0.60, 299.0(O_2)	301
1100 - 2400	0.0054	1.50	0.67, 552.2(O_2)	301
1100 - 2400	0.0054	1.50	0.39, 460.9(O_2)	301
1100 - 2400	0.0054	1.50	0.32, 460.8(O_2)	301
1100 - 2400	0.0054	0.25	2.80, 247.9(N_2)	301
1100 - 2400	0.0054	0.25	2.78, 352.1(N_2)	301
1100 - 2400	0.0054	0.25	2.82, 454.5(N_2)	301
1100 - 2400	0.0054	0.25	2.84, 547.8(N_2)	301
1100 - 2400	0.0054	0.25	2.70, 275.2(air)	301
1100 - 2400	0.0054	0.25	2.75, 349.7(air)	301
1100 - 2400	0.0054	0.25	2.80, 468.2(air)	301
1100 - 2400	0.0054	0.25	2.83, 546.6(air)	301
*590 - 2600	0.0053	25	0.00	295
590 - 2600	0.0053	25	0.545	295
590 - 2600	0.0053	73	0.486	295
590 - 2600	0.0053	193	0.479	295
590 - 2600	0.0053	433	0.484	295
590 - 2600	0.0053	433	4.83	295
590 - 2600	0.0053	193	4.83	296
590 - 2600	0.0053	25	4.85	296
590 - 2600	0.0053	73	4.86	296

* $H_2{}^{16}O$ absorptions observed were due to 0.018 Torr $H_2{}^{16}O$ pressure in the vacuum tank which enclosed the FTS and atmospheric $H_2{}^{16}O$ (total pressure was 600 Torr) in the spaces between the IR source and entry to the tank. The open spaces were purged with cooled N_2. The optical path of the open spaces was approximately 5.5 m.

absorption path lengths, pressures, and temperatures. Sample temperatures were inferred from readings of thermistor probes in thermal contact with the absorption cell walls, while the sample pressures were measured with a Baratron gauge with a 1- or 10- or 1000-Torr pressure head. The infrared radiation from a globar source was collected onto a helium-cooled arsenic-doped silicon single element detector. Each FTS run consisted of 12 or more coadded interferograms. The signal-to-noise ratios of the spectra ranged from about 500/1 with the absorption path length at 25 m to about 130/1 with a 433-m path length. The composite interferograms were transformed into spectral data at the Kitt Peak facility.

Medium-to-strong absorptions of $H_2{}^{16}O$ contained added contributions from a combination of narrow, low-pressure absorptions as a result of a small amount of water vapor and CO_2 ($\approx$200 μm total pressure) in the vacuum tank that enclosed the FTS and air-broadened $H_2{}^{16}O$ absorptions that were caused by the $H_2{}^{16}O$ content in the open spaces between the infrared source and the vacuum tank. These added, narrow, contributions were useful in the measurements of the stronger lines using the scan, listed in Table 1, with the 6-m cell evacuated.

The optical path from the 6-m cell to the vacuum tank which enclosed the FTS contained a 2.39-m-long evacuated cell and several compartments which were purged with dry N_2. The optical path from the exit of the 6-m cell to the entrance to the vacuum tank was about 5.5 m. This setup greatly reduced interference from the H_2O spectral absorptions due to room air. For one of the runs (73 m path, 0.486 Torr pressure) a small amount of N_2O (0.2 Torr pressure) was added to the 2.39-m cell for purposes of frequency calibration below 1200 cm^{-1}. The residual room air in the vacuum tank also contained enough CO_2 so that the strong ν_2 lines were observed in all the spectra below 700 cm^{-1} and these lines were also used for frequency calibration. The measured line positions were calibrated and corrected by reference to accurate $H_2{}^{16}O$ frequencies (*1*, *2*) for the region above 1200 cm^{-1} and N_2O (*15*) and CO_2 (*16*) positions covering observations below 1200 cm^{-1}.

A computer program of nonlinear least squares was used to derive experimental values of line positions, strengths, and linewidths from the spectral data listed in Table 1. This technique has been used in several previous studies [e.g., Refs. (*1*)–(*3*) and (*10*)].

All of the runs listed in Table 1 were used to obtain line-strengths and those with the shorter path lengths (0.25–1.75 m)

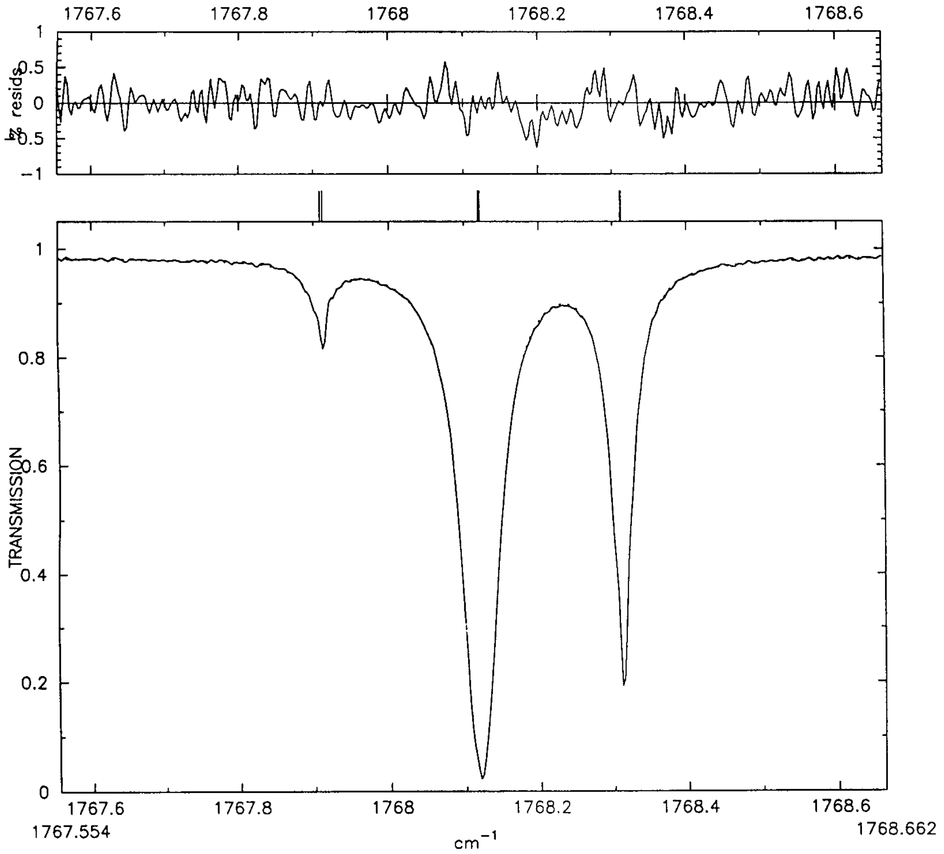

FIG. 1. Unapodized observed and synthetic spectra of $H_2{}^{16}O$. The features are caused by a narrow, low-pressure (vacuum tank H_2O) $H_2{}^{16}O$ feature superimposed on the O_2-broadened counterpart. The partial pressures representing the broadened features are 0.67 Torr (H_2O) and 552.2 Torr (O_2) and the path length is 1.5 m. The observed spectrum is overlaid with the respective synthetic spectrum, and the residue plot, shown in the upper portion, gives the percent differences between the observed and synthetic spectra.

were used to derive the experimental values of the stronger lines of $H_2{}^{16}O$. In an earlier study by this author (*1*), the strengths of the stronger lines were inferred from pressure-broadened $H_2{}^{16}O$ absorptions due to room air in the optical path. The short path runs given in Table 1 represent data obtained with two stainless steel absorption cells (1.5 and 0.25 m in length) that were placed between the globar source and the vacuum tank which encloses the FTS. All portions of the external path and the source enclosures were evacuated by using some newly installed apparatus, thus eliminating room air in the optical path.

The empty cell run given in Table 1 (*1*) with a path of 25 m and 0.0 pressure was used to determine the effective H_2O absorption amount due to the low-pressure content in the vacuum tank. By this procedure, it was determined that only the stronger lines with linestrength values $\geq 10^{-2}$ cm^{-2}/atm were observed in the spectra. Therefore two line positions for a given H_2O absorption were input to the NLLS program for the stronger lines: one representing the pressure-broadened contribution and the other for the low-pressure feature from the vacuum tank. It was not necessary to include two input lines in the NLLS routine for the 6-m cell runs because the vacuum tank contributions were dwarfed by their respective long path counterparts. Also linestrength measurements from the 6-m cell runs of the stronger lines were not used in the analysis. Therefore the observed strengths of the stronger lines were determined from the pressure-broadened runs and the strongest transitions from the foreign-broadened runs. The usable linestrength values derived from the self-broadened runs were for transitions with strengths between 10^{-3} and 0.12 cm^{-2}/atm whereas for the foreign-broadened runs, only lines with strengths ≥ 0.07 cm^{-2}/atm were reliable.

Examples of the NLLS analysis of the foreign-broadening runs are displayed in Figs. 1–4. Figs. 1 and 2 show $H_2{}^{16}O$ lines broadened by O_2 and Figs. 3 and 4 show $H_2{}^{16}O$ lines broadened by dry air. The low-pressure contributions appear on top of the pressure-broadened counterparts. The observed spectra are overlaid with the respective synthetic spectra and the residual plots are shown in the upper portions of the figures and give the percent differences between observed and computed spectra. For a given transition, the linewidth parameter for O_2 broadening is approximately 55% of that for air broadening and this effect is apparent by comparing the O_2-broadened lines displayed in Figs. 1 and 2 with the air-broadened lines shown in Figs. 3 and 4. Inspection of

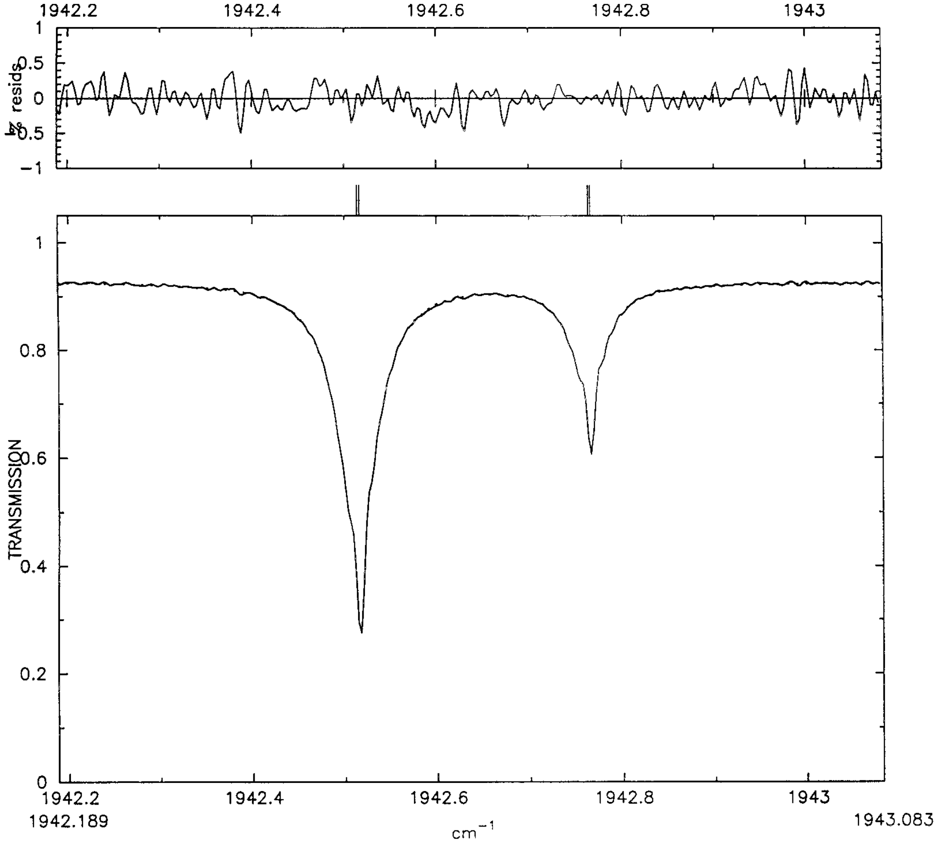

FIGURE 2

Figs. 1 and 2 show the pressure-broadened components only a little wider than the Doppler-width counterparts. However the respective parameters of the two components were easily determined from the operation of the NLLS program and therefore accurate pressure-broadened parameters (linestrength, linewidth, and frequency-shifted position) were obtained from the $H_2O + O_2$ spectra.

3. FREQUENCY MEASUREMENTS

The rotational energy levels derived in my earlier work (*1*) for the (000) and (010) vibrational states of $H_2{}^{16}O$ are, on the average, accurate for the majority of the levels given but suspect for a few of the higher J and/or K_a term values. The frequency measurements from the present set, especially the transitions of the (000)–(000) band above 590 cm^{-1}, have provided the necessary information to obtain more accurate values for these suspect term values for the ground state. These data also provided additional energy level values not included in the earlier work (*1*). Recent measurements and analysis of hot water laboratory emission spectra (*6, 7*) covering the 370–930 cm^{-1} region and further studies of hot water in sunspot and laboratory emission spectra (*8, 9*) (to 1011 cm^{-1}) in this region have provided accurate information on the quantum assignments of the observed transition frequencies which encompassed a tremendous amount of $H_2{}^{16}O$ transitions involving vibrational transitions ranging from the (000)–(000) band upward and beyond the (001)–(001) band with J values ≤ 38. The composite compilation of the laboratory data listings were obtained by this author through the internet. Also obtained in this fashion was a listing of their (*6–9*) derivation of the energy levels for the several vibrational bands involved in the observed transitions. The sunspot $H_2{}^{16}O$ frequencies used in the present analysis were taken from Ref. (*9*).

Over 200 transitions in the (000)–(000) band and a few frequencies in the (010)–(010) and (010)–(000) bands given in the emission listings (*6–9*) were also measured in this study and a comparison of the line positions indicates that the emission values are, on the average, higher than those in this work by 4.5×10^{-4} cm^{-1} with an uncertainty in their values of $\pm 3.2 \times 10^{-4}$ cm^{-1}, and in a few cases, the differences exceeded ± 0.002 cm^{-1}. Their laboratory data (*6, 7*) were obtained by flowing water vapor through a 1.2-m hot cell with the pressure maintained at ≈ 15 Torr. Pressure-induced frequency shifts could be as large as ± 0.0006 cm^{-1} (*12*) at this pressure for many of the observed transitions which may, in part, explain the rather large derived uncertainty (± 0.00032 cm^{-1}) in their values.

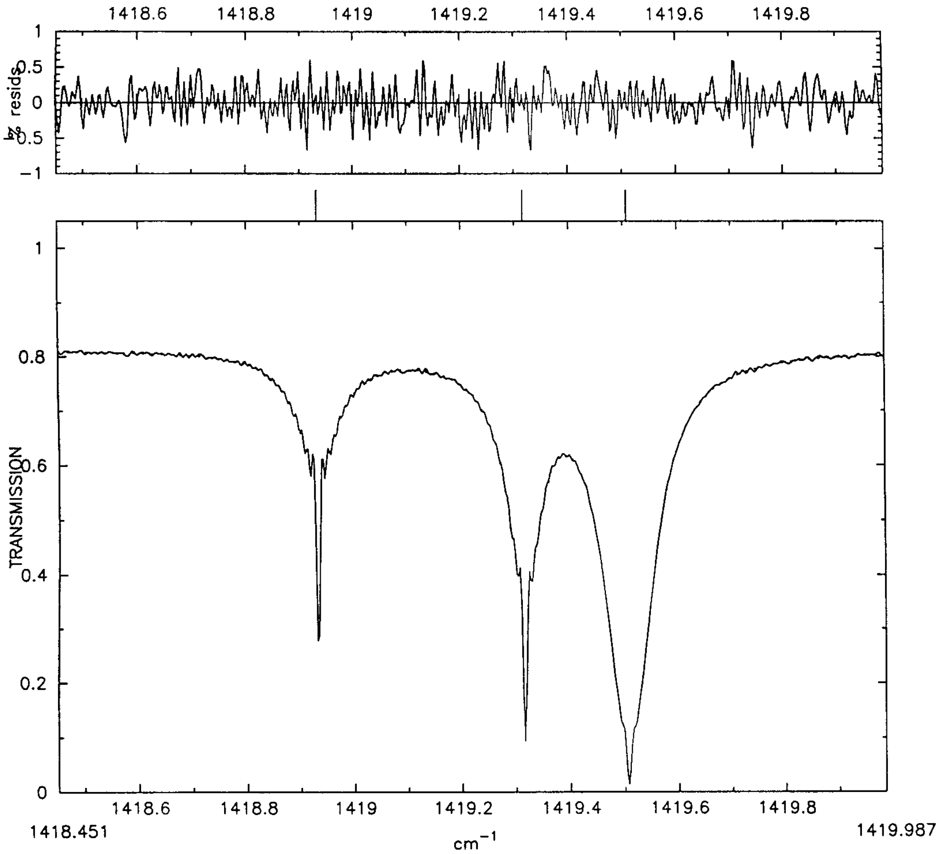

FIG. 3. Unapodized observed and synthetic spectra of $H_2{}^{16}O$. The features are caused by a narrow, low-pressure (vacuum tank H_2O) $H_2{}^{16}O$ feature superimposed on the air-broadened counterpart. The partial pressures representing the broadened features are 2.75 Torr (H_2O) and 349.7 Torr (air) and the path length is 0.25 m. The observed spectrum is overlaid with the respective synthetic spectrum, and the residue plot, shown in the upper portion, gives the percent differences between the observed and synthetic spectra.

Pearson *et al.* (*4*) measured the frequencies of 30 millimeter- and submillimeter-wave transitions of $H_2{}^{16}O$ between 100 and 600 GHz (3.3–20.0 cm^{-1}) which included transitions of the (000)–(000), (010)–(010), (020)–(020), (100)–(100), and (001)–(001) bands. This represents almost the same number of measurements made in previous studies covering frequencies only in the (000)–(000) and (010)–(010) bands and these previous results were used in my earlier analysis (*1*) of the (000) and (010) vibrational states. Pearson *et al.* (*4*) list all of the measurements (69 in all) with references to the previous studies. In all, Pearson *et al.* (*4*) give a measurement uncertainty of about 100 kHz (0.3×10^{-5} cm^{-1}).

Matsushima *et al.* (*5*) measured 137 pure rotational transitions in the (000)–(000) band from 0.5 to 5 THz (18.5–162.4 cm^{-1}) at high accuracy using a tunable far-infrared spectrometer. Six of the transitions that they measured were also measured by microwave techniques (*4*) and the agreement between the two sets of measurements for these six lines is excellent: on the average, the difference is less than 0.14 MHz (0.5×10^{-5} cm^{-1}) in magnitude. The combination of the microwave and far-IR data for the ground state includes transitions that involve all rotational levels with $J \leq 7$ and the majority of the levels with $J = 8$ and $j = 9$ and several with $J = 10$.

The measurements obtained in the present study for $H_2{}^{16}O$ include 1288 transitions in the (010)–(000) band, 306 lines in the (000)–(000) band, and 49 frequencies in the (010)–(010) band. Also included were measurements of 75 lines in the (000)–(000) band of $H_2{}^{18}O$ and 31 lines in the (000)–(000) band of $H_2{}^{17}O$ and several measurements in the (010)–(000) bands of the two isotopic species. The measurements from the runs (bottom eight given in Table 1) were weighted and then averaged with measurements made in earlier studies (*1, 10*) incorporated in this analysis. In all, the transition frequencies were determined to an absolute accuracy of 0.0001 cm^{-1} or better for the majority of the lines with an uncertainty in the precision of the measurements of 6×10^{-5} cm^{-1}.

4. ENERGY LEVELS

A. $H_2{}^{16}O$

The procedure used here to derive the energy levels from the measured frequencies is the same as that outlined in Ref. (*1*).

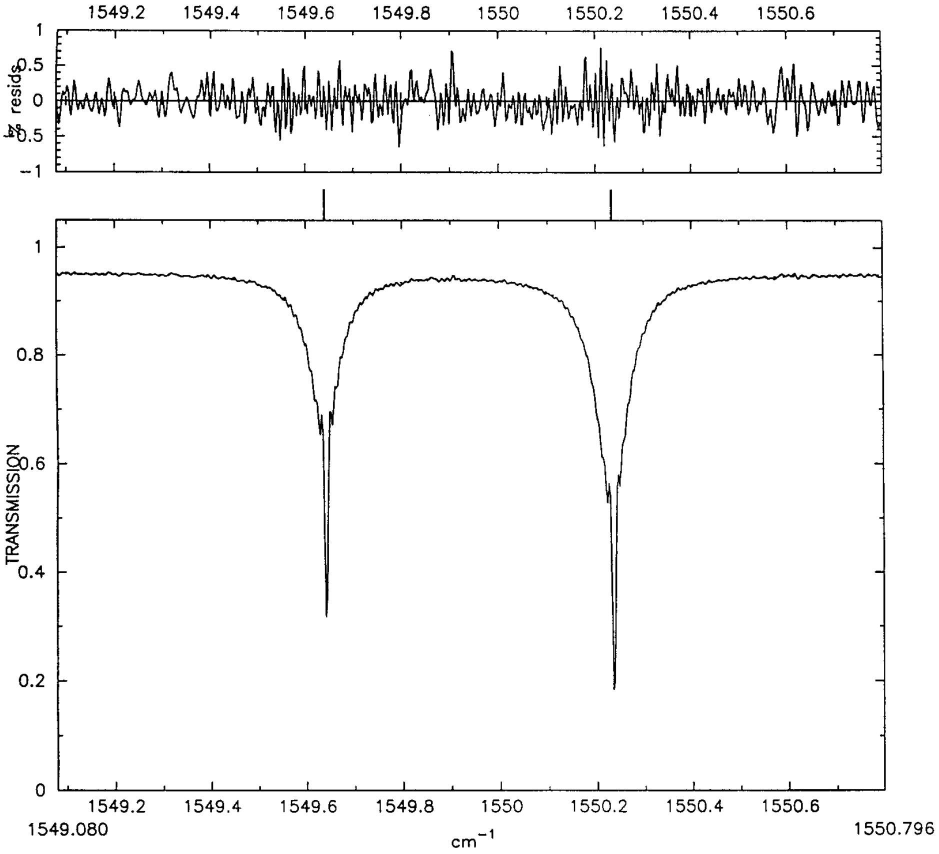

FIG. 4. Unapodized observed and synthetic spectra of $H_2{}^{16}O$. The features are caused by a narrow, low-pressure (vacuum tank H_2O) $H_2{}^{16}O$ feature superimposed on the air-broadened counterpart. The partial pressures representing the broadened features are 2.70 Torr (H_2O) and 275.2 Torr (air) and the path length is 0.25 m. The observed spectrum is overlaid with the respective synthetic spectrum, and the residue plot, shown in the upper portion, gives the percent differences between the observed and synthetic spectra.

Initially, combination difference frequencies (CDFs) in the ground state were determined from measurements in the (010)–(000) band and were used in conjunction with (000)–(000) band measurements. In the earlier report (*1*) the lowest J levels of the ground state were fitted together with use of the Hamiltonian that is caused by Watson (*17*) containing terms up to and including K^{10} and those term values derived by this technique were used in this work. These levels include the $J = 1$ levels and the 2 1 1 level. The other levels were determined by the method of adding to the CDFs and the pure rotational transition frequencies the determined values of the lower rotational level. These results were weighted and averaged with the highest weight given to the microwave and far-IR measurements. The majority of the levels with $j \leq 9$ and five levels for $J = 10$ were derived by this method using only microwave (*4*) and far-IR (*5*) observations because of their superior accuracy, and these results were given uncertainties based on their respective estimated accuracies which, over all, were better than 1.1×10^{-5} cm^{-1}. By this procedure, 24 lines in the (000)–(000) band measured in the present study and many CDFs were not included in the analysis. The remaining analysis of the ground state levels included measurements from this study as well as emission data (*6–9*) involving the (000) state. The emission observed frequencies were modified to the calibration used in this study: reducing those values by 4.5×10^{-4} cm^{-1}. Also, because of their rather high uncertainties, $\pm 3.2 \times 10^{-4}$ cm^{-1}, the emission data were only used in the analysis when the upper rotational levels to be derived were sparse in the other data.

After the ground state term values and associated estimated uncertainties were derived, the rotational levels in the (010) state were determined from the (010)–(000) and (010)–(010) band measurements by adding to each measured transition frequency, the appropriate lower state energy level. These results were weighted and averaged for each level. As was the case for the ground state analysis, the highest weight was given to the microwave (*4*) measurements and the emission (*6–9*) data were only included when other measurements of the desired levels were scarce.

B. $H_2{}^{17}O$ and $H_2{}^{18}O$

The same procedure use for the $H_2{}^{16}O$ analysis was followed for the analysis of the rare oxygen species using frequency mea-

TABLE 2

Energy Levels of the (000) and (010) States of $H_2{}^{16}O$, $H_2{}^{17}O$, and $H_2{}^{18}O$ in cm^{-1}[a]

			(000)			(010)		
J	K_a	K_c	$H_2{}^{16}O$	$H_2{}^{17}O$	$H_2{}^{18}O$	$H_2{}^{16}O$	$H_2{}^{17}O$	$H_2{}^{18}O$
0	0	0	0.0	0.0	0.0	1594.74630(5.)	1591.32565(5.)	1588.27567(10.)
1	0	1	23.794350(.5)	23.77351(2.)	23.754902(.5)	1618.55716(6.)	1615.11512(2.)	1612.04601(2.)
1	1	1	37.137118(.5)	36.93111(2.)	36.748647(.5)	1634.96709(4.)	1631.31501(3.)	1628.06006(3.)
1	1	0	42.371743(.5)	42.18694(2.)	42.023428(.5)	1640.50584(2.)	1636.87274(2.)	1633.63471(3.)
2	0	2	70.090805(.5)	70.00467(2.)	69.927440(.5)	1664.96455(2.)	1661.45949(4.)	1658.33390(3.)
2	1	2	79.496378(.8)	79.22734(2.)	78.988654(.5)	1677.06142(2.)	1673.34734(2.)	1670.03711(3.)
2	1	1	95.175932(.5)	94.97054(2.)	94.788645(.5)	1693.64994(1.)	1689.99276(2.)	1686.73337(3.)
2	2	1	134.901638(.8)	134.14527(3.)	133.475798(.7)	1742.30564(4.)	1738.02754(2.)	1734.21852(3.)
2	2	0	136.163914(.5)	135.43118(2.)	134.783115(.7)	1743.48633(1.)	1739.22848(3.)	1735.43774(3.)
3	0	3	136.761650(.8)	136.53762(2.)	136.336669(.7)	1731.89669(3.)	1728.26026(2.)	1725.01689(4.)
3	1	3	142.278479(.5)	141.90241(2.)	141.568060(.7)	1739.48369(1.)	1735.66575(2.)	1732.26277(2.)
3	1	2	173.365800(.8)	173.11009(2.)	172.882910(.7)	1772.41349(5.)	1768.70419(2.)	1765.39801(3.)
3	2	2	206.301422(.5)	205.48182(2.)	204.755913(.7)	1813.78756(1.)	1809.44407(2.)	1805.57671(2.)
3	2	1	212.156358(.8)	211.43578(1.)	210.799282(.7)	1819.33510(2.)	1815.07905(3.)	1811.29062(4.)
3	3	1	285.219338(.5)	283.56166(3.)	282.09458(3.)	1907.45138(2.)	1902.15935(2.)	1897.45282(2.)
3	3	0	285.418566(.8)	283.76776(3.)	282.30709(3.)	1907.61573(2.)	1902.32895(2.)	1897.62724(2.)
4	0	4	222.052755(.8)	221.62081(2.)	221.23401(1.)	1817.45115(5.)	1813.61195(4.)	1810.18732(2.)
4	1	4	224.838378(.8)	224.30423(1.)	223.828555(.7)	1821.59680(2.)	1817.62639(4.)	1814.08716(4.)
4	1	3	275.497035(.5)	275.13055(2.)	274.80321(2.)	1875.46966(2.)	1871.65496(4.)	1868.25385(3.)
4	2	3	300.362283(.8)	299.43892(2.)	298.62018(1.)	1908.01630(2.)	1903.56907(3.)	1899.60894(2.)
4	2	2	315.779529(.5)	315.07849(1.)	314.45946(1.)	1922.90108(2.)	1918.65776(3.)	1914.88091(2.)
4	3	2	382.516883(.8)	380.80593(4.)	379.29162(4.)	2004.81567(3.)	1999.46329(2.)	1994.70331(5.)
4	3	1	383.842507(.5)	382.17599(4.)	380.70252(3.)	2005.91700(1.)	2000.59878(2.)	1995.87013(2.)
4	4	1	488.107689(.8)	485.20903(2.)	482.64357(2.)	2129.59918(2.)	2122.93237(5.)	2117.00849(4.)
4	4	0	488.134159(.8)	485.23684(2.)	482.67262(2.)	2129.61861(3.)	2122.95273(6.)	2117.02971(2.)
5	0	5	325.347903(.8)	324.66099(2.)	324.04675(3.)	1920.76651(3.)	1916.67358(4.)	1913.02264(3.)
5	1	5	326.625464(.5)	325.88023(3.)	325.21574(1.)	1922.82904(3.)	1918.65480(3.)	1914.93352(2.)
5	1	4	399.457515(.8)	398.87940(2.)	398.36052(3.)	2000.86301(2.)	1996.85377(5.)	1993.27689(5.)
5	2	4	416.208734(.5)	415.12802(2.)	414.16819(2.)	2024.15264(1.)	2019.55169(3.)	2015.45396(3.)
5	2	3	446.510667(.5)	445.79344(2.)	445.15858(4.)	2053.96866(3.)	2049.71212(4.)	2045.92267(2.)
5	3	3	503.968093(.8)	502.17968(2.)	500.59627(1.)	2126.40768(3.)	2120.97240(7.)	2116.13858(2.)
5	3	2	508.812047(.8)	507.17439(2.)	505.72884(2.)	2130.49428(2.)	2125.17883(3.)	2120.45465(2.)
5	4	2	610.114421(.8)	607.15929(2.)	604.54422(3.)	2251.69528(3.)	2244.95965(6.)	2238.97495(2.)
5	4	1	610.341157(.8)	607.39740(2.)	604.79294(3.)	2251.86248(2.)	2245.13452(6.)	2239.15705(4.)
5	5	1	742.073013(.8)	737.62061(9.)	733.67939(2.)	2406.14089(2.)	2397.77881(5.)	2390.35358(4.)
5	5	0	742.076282(.8)	737.62415(9.)	733.68310(7.)	2406.14305(3.)	2397.78115(3.)	2390.35608(3.)
6	0	6	446.696587(.8)	445.71922(5.)	444.84623(2.)	2041.78049(2.)	2037.39776(4.)	2033.48870(3.)
6	1	6	447.252348(.5)	446.24496(2.)	445.34623(1.)	2042.75329(3.)	2038.32509(5.)	2034.37691(6.)
6	1	5	542.905774(.5)	541.99683(3.)	541.18017(3.)	2146.26372(2.)	2141.94454(4.)	2138.08859(2.)
6	2	5	552.911385(.5)	551.60938(2.)	550.45085(2.)	2161.28604(4.)	2156.47142(3.)	2152.18212(2.)
6	2	4	602.773486(.5)	601.96080(7.)	601.23786(1.)	2211.19059(2.)	2206.85500(3.)	2202.99275(3.)
6	3	4	648.978686(.8)	647.07220(2.)	645.38263(3.)	2271.71221(2.)	2266.15787(2.)	2261.21753(2.)
6	3	3	661.548903(.5)	659.98679(3.)	658.61010(3.)	2282.58956(3.)	2277.32399(6.)	2272.64614(2.)
6	4	3	756.724776(.8)	753.70510(2.)	751.03301(2.)	2398.38146(3.)	2391.56739(3.)	2385.51357(3.)
6	4	2	757.780178(.8)	754.81181(8.)	752.18752(3.)	2399.16545(2.)	2392.38680(7.)	2386.36587(3.)
6	5	2	888.598735(.8)	884.07779(9.)	880.07636(4.)	2552.85723(2.)	2544.40996(5.)	2536.90967(2.)
6	5	1	888.632640(.8)	884.11390(6.)	880.11463(3.)	2552.87968(2.)	2544.43388(10.)	2536.93489(4.)
6	6	1	1045.057939(.8)	1038.76539(15.)	1033.19414(6.)	2733.96268(3.)	2723.62232(10.)	2714.44436(9.)
6	6	0	1045.058330(.8)	1038.76595(30.)	1033.19456(8.)	2733.96292(3.)	2723.62280(40.)	2714.44446(10.)
7	0	7	586.243542(.8)	584.94089(3.)	583.77780(2.)	2180.64288(3.)	2175.93741(5.)	2171.74074(3.)
7	1	7	586.479178(.8)	585.16194(2.)	583.98653(2.)	2181.08986(3.)	2176.36028(4.)	2172.14324(1.)
7	1	6	704.214044(.5)	702.88597(3.)	701.69433(3.)	2309.73018(4.)	2304.99914(3.)	2300.77427(4.)
7	2	6	709.608206(.5)	708.01636(3.)	706.59783(2.)	2318.53988(3.)	2313.44576(2.)	2308.90606(4.)
7	2	5	782.409819(.5)	781.37727(2.)	780.45286(2.)	2392.59252(2.)	2388.07275(4.)	2384.04199(3.)
7	3	5	816.694228(.5)	814.61075(3.)	812.76176(3.)	2439.95442(3.)	2434.22907(2.)	2429.13504(3.)
7	3	4	842.356585(.5)	840.86487(5.)	839.54954(2.)	2462.87526(2.)	2457.67610(3.)	2453.05763(2.)
7	4	4	927.743894(.8)	924.64153(6.)	921.89590(2.)	2569.50794(2.)	2562.59955(2.)	2556.46217(4.)
7	4	3	931.237097(.8)	928.29587(3.)	925.69983(3.)	2572.13915(2.)	2565.34541(5.)	2559.31399(2.)
7	5	3	1059.646645(.8)	1055.05411(7.)	1050.99030(3.)	2724.04142(3.)	2715.50255(3.)	2707.92173(3.)
7	5	2	1059.835444(.8)	1055.25530(6.)	1051.20326(3.)	2724.16709(3.)	2715.63588(8.)	2708.06223(2.)
7	6	2	1216.189759(.8)	1209.81339(4.)	1204.16951(4.)	2905.43060(4.)	2894.98645(10.)	2885.71721(5.)
7	6	1	1216.194499(.8)	1209.81842(9.)	1204.17496(2.)	2905.43346(2.)	2894.98966(6.)	2885.72063(10.)
7	7	1	1394.81415(1.)	1386.41873(20.)	1378.98643(14.)	3109.91150(4.)	3097.34225(45.)	3086.18826(13.)
7	7	0	1394.81420(1.)	1386.41898(9.)	1378.98643(14.)	3109.91161(5.)	3097.34225(45.)	3086.18826(13.)

[a] The values given within parentheses are estimated uncertainties in the last digits.

TABLE 2—*Continued*

			(000)			(010)		
J	K_a	K_c	$H_2{}^{16}O$	$H_2{}^{17}O$	$H_2{}^{18}O$	$H_2{}^{16}O$	$H_2{}^{17}O$	$H_2{}^{18}O$
8	0	8	744.063655(.8)	742.39857(4.)	740.91235(3.)	2337.46325(2.)	2332.40026(10.)	2327.88508(5.)
8	1	8	744.162658(.8)	742.49085(5.)	740.99874(3.)	2337.66680(1.)	2332.59152(3.)	2328.06602(4.)
8	1	7	882.890321(.8)	881.09903(4.)	879.49487(3.)	2490.35404(2.)	2485.15129(4.)	2480.50570(6.)
8	2	7	885.600207(.8)	883.65191(2.)	881.91415(6.)	2495.16582(2.)	2489.72633(3.)	2484.87728(3.)
8	2	6	982.911707(.8)	981.49596(4.)	980.22238(3.)	2595.81290(4.)	2590.96402(7.)	2586.63359(3.)
8	3	6	1006.115929(.8)	1003.78133(3.)	1001.70586(2.)	2630.19257(3.)	2624.22928(3.)	2618.92134(3.)
8	3	5	1050.157656(.5)	1048.65714(4.)	1047.32865(5.)	2670.78960(5.)	2665.60912(4.)	2661.00404(4.)
8	4	5	1122.708530(.8)	1119.48803(4.)	1116.63623(2.)	2764.69742(2.)	2757.66597(3.)	2751.41854(5.)
8	4	4	1131.775561(.8)	1128.93814(3.)	1126.43916(2.)	2771.69012(5.)	2764.94432(3.)	2758.96016(7.)
8	5	4	1255.166746(.8)	1250.49869(6.)	1246.36855(10.)	2919.63292(2.)	2910.99637(9.)	2903.32966(4.)
8	5	3	1255.911532(.8)	1251.29115(4.)	1247.20616(5.)	2920.13200(4.)	2911.52516(7.)	2903.88643(3.)
8	6	3	1411.611435(.8)	1405.14811(16.)	1399.42806(4.)	3101.12382(5.)	3090.56812(7.)	3081.20101(4.)
8	6	2	1411.641877(.8)	1405.18093(4.)	1399.46336(4.)	3101.14216(5.)	3090.58788(10.)	3081.22215(10.)
8	7	2	1590.69006(2.)	1582.19624(16.)	1574.67800(25.)	3306.29516(6.)	3293.60285(15.)	3282.34196(20.)
8	7	1	1590.69069(2.)	1582.19672(16.)	1574.67845(15.)	3306.29552(3.)	3293.60356(10.)	3282.34264(24.)
8	8	1	1789.04284(4.)	1778.30779(25.)	1768.80148(15.)	3530.95752(6.)	3515.93481(20.)	3502.60781(20.)
8	8	0	1789.04284(4.)	1778.30779(25.)	1768.80148(15.)	3530.95752(6.)	3515.93481(20.)	3502.60781(20.)
9	0	9	920.168343(.8)	918.10200(2.)	916.25779(3.)	2512.28282(2.)	2506.82584(4.)	2501.95936(4.)
9	1	9	920.209983(.8)	918.14050(8.)	916.29360(5.)	2512.37563(2.)	2506.91246(15.)	2502.04083(3.)
9	1	8	1079.079575(.8)	1076.80099(3.)	1074.76308(4.)	2688.07989(3.)	2682.37533(3.)	2677.28341(3.)
9	2	8	1080.385427(.8)	1078.02032(8.)	1075.90952(4.)	2690.59359(4.)	2684.74692(4.)	2679.53359(3.)
9	2	7	1201.921495(.8)	1199.96295(3.)	1198.19966(2.)	2818.39806(3.)	2813.05657(7.)	2808.28033(5.)
9	3	7	1216.231248(.8)	1213.56231(4.)	1211.18576(3.)	2841.43075(2.)	2835.15251(4.)	2829.56108(2.)
9	3	6	1282.919103(.8)	1281.26845(6.)	1279.79767(3.)	2904.67039(3.)	2899.39855(9.)	2894.70566(3.)
9	4	6	1340.884869(.8)	1337.48949(3.)	1334.47935(4.)	2983.32302(4.)	2976.12209(3.)	2969.72205(4.)
9	4	5	1360.235330(.5)	1357.55585(8.)	1355.19916(8.)	2998.76631(4.)	2992.13633(8.)	2986.25913(12.)
9	5	5	1474.980775(.8)	1470.22554(5.)	1466.01837(14.)	3139.47578(3.)	3130.73149(4.)	3122.96952(6.)
9	5	4	1477.297357(.8)	1472.68499(9.)	1468.61221(8.)	3141.04598(3.)	3132.39268(6.)	3124.71649(7.)
9	6	4	1631.245475(.8)	1624.69354(6.)	1618.89634(7.)	3320.92978(3.)	3310.25716(4.)	3300.78715(7.)
9	6	3	1631.383001(1.0)	1624.84233(12.)	1619.05587(10.)	3321.01334(9.)	3310.34699(9.)	3300.88304(3.)
9	7	3	1810.58328(3.)	1801.98494(16.)	1794.37475(12.)	3526.62488(4.)	3513.80024(18.)	3502.42285(10.)
9	7	2	1810.58791(2.)	1801.99017(9.)	1794.38045(8.)	3526.62745(3.)	3513.80312(10.)	3502.42601(10.)
9	8	2	2009.80498(6.)	1998.95625(19.)	1989.35195(10.)	3752.41595(10.)	3737.25325(30.)	3723.80404(12.)
9	8	1	2009.80510(2.)	1998.95635(19.)	1989.35195(10.)	3752.41622(5.)	3737.25325(30.)	3723.80404(12.)
9	9	1	2225.46914(4.)	2212.16617(300.)	2200.40535(25.)	3994.26025(9.)	3976.58649(25.)	3960.90900(50.)
9	9	0	2225.46914(4.)	2212.16617(300.)	2200.40535(25.)	3994.26025(9.)	3976.58649(25.)	3960.90900(50.)
10	0	10	1114.53218(3.)	1112.02499(10.)	1109.78708(4.)	2705.09685(4.)	2699.20781(4.)	2693.95617(5.)
10	1	10	1114.54987(2.)	1112.04116(5.)	1109.80211(3.)	2705.13959(3.)	2699.24745(4.)	2693.99338(4.)
10	1	9	1293.01816(4.)	1290.22818(6.)	1287.73485(3.)	2903.14605(3.)	2896.91783(15.)	2891.35977(3.)
10	2	9	1293.63404(1.)	1290.79853(3.)	1288.26735(2.)	2904.42833(3.)	2898.11899(4.)	2892.49216(2.)
10	2	8	1437.96860(2.)	1435.36731(8.)	1433.02899(2.)	3058.39842(5.)	3052.43092(4.)	3047.09238(4.)
10	3	8	1446.12824(1.)	1443.04107(4.)	1440.28806(5.)	3072.72635(5.)	3066.05164(3.)	3060.10398(3.)
10	3	7	1538.14948(2.)	1536.15667(6.)	1534.36837(5.)	3162.25889(5.)	3156.73632(6.)	3151.80973(8.)
10	4	7	1581.33597(2.)	1577.68835(5.)	1574.44957(4.)	3224.54657(5.)	3217.11097(11.)	3210.49931(6.)
10	4	6	1616.45303(3.)	1613.90094(7.)	1611.65357(8.)	3253.73798(4.)	3247.24322(16.)	3241.48623(5.)
10	5	6	1718.71880(2.)	1713.84955(10.)	1709.53976(15.)	3383.26542(3.)	3374.39338(8.)	3366.51786(2.)
10	5	5	1724.70541(4.)	1720.18418(12.)	1716.19952(15.)	3387.40068(3.)	3378.75881(4.)	3371.09898(4.)
10	6	5	1874.97300(5.)	1868.33073(12.)	1862.45488(5.)	3564.70504(4.)	3553.91092(10.)	3544.33447(6.)
10	6	4	1875.46186(5.)	1868.85882(9.)	1863.01980(15.)	3565.00356(4.)	3554.23163(11.)	3544.67620(5.)
10	7	4	2054.34525(3.)	2045.63885(12.)	2037.93395(10.)	3770.71136(5.)	3757.74618(8.)	3746.24537(3.)
10	7	3	2054.36868(3.)	2045.66456(7.)	2037.96200(15.)	3770.72451(6.)	3757.76049(15.)	3746.26098(15.)
10	8	3	2254.28383(5.)	2243.31375(45.)	2233.60265(20.)	3997.50835(10.)	3982.19397(40.)	3968.60945(40.)
10	8	2	2254.28442(4.)	2243.31440(80.)	2233.60315(30.)	3997.50855(8.)	3982.19397(40.)	3968.61025(40.)
10	9	2	2471.25497(2.)	2457.83590(50.)	2445.95450(60.)	4240.94214(6.)	4223.11065(40.)	4208.52029(20.)
10	9	1	2471.25497(2.)	2457.83590(50.)	2445.95450(60.)	4240.94214(6.)	4223.11065(40.)	4208.52029(20.)
10	10	1	2701.88862(6.)	2685.84239(90.)	2671.62985(100.)	4497.19262(15.)		4467.82595(300.)
10	10	0	2701.88862(6.)	2685.84239(90.)	2671.62985(100.)	4497.19262(15.)		4467.82595(300.)
11	0	11	1327.10996(4.)	1324.12157(8.)	1321.45434(8.)	2915.87433(3.)	2909.51494(2.)	2903.84380(5.)
11	1	11	1327.11762(2.)	1324.12830(20.)	1321.46052(5.)	2915.89430(4.)	2909.53331(6.)	2903.86092(3.)
11	1	10	1524.84791(2.)	1521.51755(9.)	1518.54258(5.)	3135.76472(1.)	3128.98788(6.)	3122.94139(5.)
11	2	10	1525.13599(3.)	1521.78224(6.)	1518.78799(4.)	3136.41252(2.)	3129.59052(13.)	3123.50601(9.)
11	2	9	1690.66438(3.)	1687.38292(5.)	1684.43944(4.)	3314.85561(3.)	3308.19035(10.)	3302.22942(5.)
11	3	9	1695.06865(3.)	1691.48503(12.)	1688.28644(5.)	3323.26983(5.)	3316.11966(7.)	3309.74535(10.)
11	3	8	1813.22339(2.)	1810.66703(8.)	1808.36235(7.)	3441.03957(3.)	3435.06637(10.)	3429.72577(3.)
11	4	8	1843.02965(2.)	1839.03757(10.)	1835.48680(20.)	3487.39929(2.)	3479.64817(20.)	3472.75147(8.)
11	4	7	1899.00816(5.)	1896.45521(8.)	1894.19577(6.)	3535.87050(4.)	3529.44342(10.)	3523.74055(5.)
11	5	7	1985.78490(5.)	1980.75352(18.)	1976.29723(11.)	3650.50913(5.)	3641.47384(40.)	3633.45155(8.)

TABLE 2—*Continued*

			(000)			(010)		
J	K_a	K_c	$H_2{}^{16}O$	$H_2{}^{17}O$	$H_2{}^{18}O$	$H_2{}^{16}O$	$H_2{}^{17}O$	$H_2{}^{18}O$
11	5	6	1998.99530(4.)	1994.66386(7.)	1990.85680(10.)	3659.90403(3.)	3651.36020(8.)	3643.79532(8.)
11	6	6	2142.59770(2.)	2135.85851(10.)	2129.89782(10.)	3832.25183(4.)	3821.33008(40.)	3811.64162(10.)
11	6	5	2144.04633(3.)	2137.41981(15.)	2131.56620(15.)	3833.14442(3.)	3822.28735(40.)	3812.68000(300.)
11	7	5	2321.81303(3.)	2312.99648(90.)	2305.19600(50.)	4038.35156(4.)	4025.23810(50.)	4013.61061(40.)
11	7	4	2321.90574(3.)	2313.09788(30.)	2305.30620(15.)	4038.40347(8.)	4025.29633(40.)	4013.67143(15.)
11	8	4	2522.26130(5.)	2511.16195(50.)	2501.45280(80.)	4265.97432(5.)	4250.85300(300.)	4236.76675(40.)
11	8	3	2522.26518(3.)	2511.16608(25.)	2501.45732(20.)	4265.97639(4.)	4250.85555(60.)	4236.76895(40.)
11	9	3	2740.42072(4.)	2726.85000(300.)	2714.86380(300.)	4510.90161(8.)		4477.87060(300.)
11	9	2	2740.42074(4.)	2726.85010(300.)	2714.86488(300.)	4510.90161(8.)		4477.87060(300.)
11	10	2	2972.82733(6.)			4769.23273(4.)		
11	10	1	2972.82733(6.)			4769.23273(4.)		
11	11	1	3216.19318(10.)			5037.34010(40.)		
11	11	0	3216.19318(10.)			5037.34010(40.)		
12	0	12	1557.84441(3.)	1554.33465(5.)	1551.20212(4.)	3144.56930(1.)	3137.70051(4.)	3131.57518(6.)
12	1	12	1557.84775(2.)	1554.33768(5.)	1551.20496(8.)	3144.57877(4.)	3137.70941(4.)	3131.58339(3.)
12	1	11	1774.61629(3.)	1770.71182(11.)	1767.22511(12.)	3386.05234(6.)	3378.69726(6.)	3372.13552(5.)
12	2	11	1774.75109(2.)	1770.83503(7.)	1767.33865(6.)	3386.37950(2.)	3378.99966(4.)	3372.41741(3.)
12	2	10	1960.20733(5.)	1956.23540(15.)	1952.67815(30.)	3587.66670(7.)	3580.27923(35.)	3573.67544(15.)
12	3	10	1962.50690(2.)	1958.35815(25.)	1954.65356(10.)	3592.42392(7.)	3584.72610(10.)	3577.86090(3.)
12	3	9	2105.86798(2.)	2102.55395(25.)	2099.56255(10.)	3738.54326(3.)	3731.75210(40.)	3725.96590(40.)
12	4	9	2124.95142(2.)	2120.51612(17.)	2116.56486(4.)	3770.87890(6.)	3762.72160(6.)	3755.45790(12.)
12	4	8	2205.65288(3.)	2202.89734(90.)	2200.43888(80.)	3843.41048(3.)	3836.95240(50.)	3831.07000(300.)
12	5	8	2275.37290(3.)	2270.10752(14.)	2265.43837(10.)	3940.51948(4.)	3931.26571(25.)	3923.04636(20.)
12	5	7	2300.68505(10.)	2296.59750(100.)	2293.01020(50.)	3959.25347(2.)	3950.91300(300.)	3943.49850(40.)
12	6	7	2433.80039(2.)	2426.94740(60.)	2420.88520(25.)	4123.28533(4.)	4112.22326(50.)	4102.04310(400.)
12	6	6	2437.50197(5.)	2430.92450(90.)	2425.12370(30.)	4125.59912(9.)	4114.53294(400.)	4104.73143(400.)
12	7	6	2612.79977(6.)	2603.86680(400.)	2595.97519(20.)	4329.32444(3.)		4303.65260(200.)
12	7	5	2613.10463(6.)	2604.20620(400.)	2596.33830(50.)	4329.49585(3.)		4303.86622(400.)
12	8	5	2813.51230(10.)	2802.27550(400.)	2792.34100(400.)	4557.54625(7.)		4527.26690(400.)
12	8	4	2813.52868(4.)		2792.35623(300.)	4557.55498(5.)		
12	9	4	3032.68981(10.)		3006.84720(400.)	4803.82047(5.)		
12	9	3	3032.69032(10.)		3006.84800(400.)	4803.82060(40.)		
12	10	3	3266.76442(3.)			5064.14116(10.)		
12	10	2	3266.76442(3.)			5064.14116(10.)		
12	11	2	3512.40486(10.)			5334.86062(100.)		
12	11	1	3512.40486(10.)			5334.86062(100.)		
12	12	1	3766.38655(40.)			5612.49312(200.)		
12	12	0	3766.38655(40.)			5612.49312(200.)		
13	0	13	1806.67004(4.)	1802.59895(6.)	1798.96549(7.)	3391.12616(2.)	3383.70953(8.)	3377.09554(5.)
13	1	13	1806.67159(2.)	1802.60001(6.)	1798.96637(7.)	3391.13066(5.)	3383.71324(19.)	3377.09926(4.)
13	1	12	2042.31058(3.)	2037.79639(5.)	2033.76570(4.)	3654.04886(3.)	3646.08238(5.)	3638.97577(11.)
13	2	12	2042.37400(6.)	2037.85408(10.)	2033.81822(5.)	3654.21514(2.)	3646.23492(5.)	3639.11710(10.)
13	2	11	2246.88475(3.)	2242.21211(6.)	2238.03200(10.)	3877.08862(4.)	3868.96959(5.)	3861.71645(5.)
13	3	11	2248.06448(3.)	2243.29282(50.)	2239.02987(35.)	3879.72071(6.)	3871.41260(20.)	3864.00035(10.)
13	3	10	2414.72341(3.)	2410.54103(300.)	2406.76989(13.)	4052.81094(3.)	4045.34602(40.)	4038.65476(8.)
13	4	10	2426.19650(4.)	2421.16090(90.)	2416.78280(50.)	4074.03868(2.)	4065.29988(400.)	4057.66655(40.)
13	4	9	2533.79322(3.)	2530.58221(300.)	2527.68887(90.)	4174.03876(3.)	4166.97610(400.)	4160.83557(200.)
13	5	9	2586.52983(3.)	2580.93620(400.)	2575.97175(50.)	4252.44845(7.)		4234.00588(400.)
13	5	8	2629.33442(3.)	2625.43660(400.)	2622.00927(40.)	4285.64751(3.)	4277.25987(400.)	4270.01836(200.)
13	6	8	2748.09954(3.)	2741.10220(400.)	2734.89597(50.)	4437.39976(5.)		
13	6	7	2756.41526(3.)	2749.99050(400.)	2744.34556(40.)	4442.71318(3.)		4421.70320(300.)
13	7	7	2927.07529(5.)		2910.04058(100.)	4643.38020(20.)		
13	7	6	2927.94138(6.)	2918.97770(400.)	2911.06346(80.)	4643.87064(3.)		
13	8	6	3127.80301(7.)		3106.38800(500.)	4871.94815(20.)		
13	8	5	3127.86186(7.)		3106.44527(200.)	4871.97898(5.)		
13	9	5	3347.78063(15.)			5119.37392(80.)		
13	9	4	3347.78329(8.)			5119.37500(80.)		
13	10	4	3583.37452(20.)			5381.55291(100.)		
13	10	3	3583.37492(20.)			5381.55291(100.)		
13	11	3	3831.17950(60.)			5654.78017(100.)		
13	11	2	3831.17950(60.)			5654.78017(100.)		
14	0	14	2073.51497(3.)	2068.84310(80.)	2064.67225(80.)	3655.48270(10.)	3647.48050(40.)	3640.34227(40.)
14	1	14	2073.51569(3.)	2068.84365(80.)	2064.67291(20.)	3655.48514(3.)	3647.48100(40.)	3640.34344(12.)
14	1	13	2327.88374(4.)	2322.71550(200.)	2318.11367(20.)	3939.74645(3.)	3931.13348(40.)	3923.44902(40.)
14	2	13	2327.91403(4.)	2322.74833(7.)	2318.13865(20.)	3939.83187(2.)	3931.21109(40.)	3923.52195(15.)
14	2	12	2550.88241(3.)	2545.49096(80.)	2540.67115(30.)	4183.38901(3.)	4174.74175(400.)	4166.66191(300.)
14	3	12	2551.48353(4.)	2546.03735(40.)	2541.17266(20.)	4184.83123(3.)	4175.95020(300.)	4167.85026(15.)

TABLE 2—*Continued*

			(000)			(010)		
J	K_a	K_c	$H_2{}^{16}O$	$H_2{}^{17}O$	$H_2{}^{18}O$	$H_2{}^{16}O$	$H_2{}^{17}O$	$H_2{}^{18}O$
14	3	11	2739.42833(3.)	2734.34220(400.)	2729.76880(300.)	4382.77967(16.)		4366.48340(300.)
14	4	11	2746.02344(3.)	2740.41880(400.)	2735.41921(20.)	4396.05147(3.)	4386.74110(400.)	4378.55929(40.)
14	4	10	2880.83417(4.)	2876.88720(400.)	2873.32307(100.)	4525.23963(9.)		
14	5	10	2918.24498(4.)	2912.22640(400.)	2906.84900(400.)	4585.34940(40.)		4565.87427(400.)
14	5	9	2983.39633(8.)			4638.35065(60.)		
14	6	9	3084.83573(6.)	3077.63530(400.)	3071.21889(400.)	4774.04405(15.)		
14	6	8	3101.44105(10.)			4785.00030(50.)		
14	7	8	3264.33751(4.)		3247.04704(70.)	4980.22302(18.)		
14	7	7	3266.51439(12.)			4981.46892(20.)		
14	8	7	3464.88738(4.)			5208.89725(50.)		
14	8	6	3465.07000(40.)			5208.99237(100.)		
14	9	6	3685.40842(10.)			5457.23704(100.)		
14	9	5	3685.41901(10.)			5457.24248(100.)		
14	10	5	3922.33083(15.)			5721.09750(60.)		
14	10	4	3922.33083(20.)			5721.09750(60.)		
14	11	4	4172.15220(60.)			5996.69061(200.)		
14	11	3	4172.15220(60.)			5996.69061(200.)		
14	12	3	4431.63822(60.)					
14	12	2	4431.63822(60.)					
14	13	2	4697.66719(200.)					
14	13	1	4697.66719(200.)					
14	14	1	4967.04078(200.)					
14	14	0	4967.04078(200.)					
15	0	15	2358.30142(4.)	2352.98827(50.)	2348.24680(50.)	3937.57154(5.)	3928.94380(50.)	3921.24790(25.)
15	1	15	2358.30170(6.)	2352.98860(100.)	2348.24680(50.)	3937.57324(20.)	3928.94380(50.)	3921.24810(25.)
15	1	14	2631.26882(5.)	2625.41069(300.)	2620.17300(400.)	4243.10965(3.)	4233.81173(40.)	4225.51964(15.)
15	2	14	2631.28362(6.)	2625.41889(500.)	2620.18800(400.)	4243.15411(3.)	4233.84680(50.)	4225.55707(40.)
15	2	13	2872.27422(5.)	2866.12270(500.)	2860.65671(30.)	4506.73386(7.)	4497.70240(400.)	4488.52332(40.)
15	3	13	2872.58046(4.)	2866.40110(500.)	2860.90850(300.)	4507.52255(10.)		4489.39005(400.)
15	3	12	3080.17871(3.)		3068.82218(30.)	4728.22116(4.)		4710.03271(400.)
15	4	12	3083.86522(10.)		3071.92687(150.)	4736.24160(35.)		
15	4	11	3244.60060(5.)	3239.67510(500.)	3235.24366(400.)	4894.58590(5.)		
15	5	11	3269.53951(5.)		3257.08115(400.)	4938.25310(60.)		
15	5	10	3360.60037(8.)	3356.48770(500.)	3352.82921(400.)	5015.70425(10.)		
15	6	10	3443.19200(7.)		3428.99980(400.)	5132.50028(100.)		
15	6	9	3472.88133(7.)			5152.96620(100.)		
15	7	9	3624.18143(6.)			5339.49000(200.)		
15	7	8	3629.09646(10.)			5342.34760(120.)		
15	8	8	3824.49837(12.)			5568.09129(100.)		
15	8	7	3824.99775(10.)			5568.35430(30.)		
15	9	7	4045.28584(15.)			5817.08046(150.)		
15	9	6	4045.32180(20.)			5817.09810(60.)		
15	10	6	4283.30580(50.)			6082.41010(200.)		
15	10	5	4283.30825(50.)			6082.41010(200.)		
15	11	5	4534.96335(60.)					
15	11	4	4534.96375(60.)					
15	12	4	4796.97025(80.)					
15	12	3	4796.97025(80.)					
15	13	3	5066.22887(60.)					
15	13	2	5066.22887(60.)					
16	0	16	2660.94520(8.)	2654.94766(300.)	2649.60481(90.)	4237.32076(10.)	4228.02847(40.)	4219.74131(20.)
16	1	16	2660.94535(12.)	2654.94779(300.)	2649.60481(90.)	4237.32083(10.)	4228.02847(40.)	4219.74131(20.)
16	1	15	2952.38650(5.)			4564.08630(7.)		4545.29570(400.)
16	2	15	2952.39365(6.)			4564.10968(5.)	4554.31785(500.)	4545.31320(400.)
16	2	14	3211.05594(10.)		3197.97600(200.)	4847.18930(35.)		
16	3	14	3211.21261(5.)		3198.07980(50.)	4847.62216(10.)		
16	3	13	3437.27732(15.)		3424.17000(400.)	5089.33655(30.)		
16	4	13	3439.30670(30.)		3425.88846(300.)	5094.08458(15.)		
16	4	12	3623.76486(10.)			5280.09573(100.)		
16	5	12	3639.53790(20.)		3625.79671(300.)	5310.23971(10.)		
16	5	11	3758.39667(10.)			5415.48887(100.)		
16	6	11	3822.24590(7.)			5512.01410(25.)		
16	6	10	3870.20154(8.)			5546.73975(100.)		
16	7	10	4006.07315(10.)			5720.72045(35.)		
16	7	9	4016.13442(10.)			5726.68746(150.)		
16	8	9	4206.33172(10.)			5949.21700(40.)		
16	8	8	4207.56190(20.)			5949.87125(200.)		

TABLE 2—*Continued*

J	K_a	K_c	(000)			(010)		
			$H_2{}^{16}O$	$H_2{}^{17}O$	$H_2{}^{18}O$	$H_2{}^{16}O$	$H_2{}^{17}O$	$H_2{}^{18}O$
16	9	8	4427.12102(35.)					
16	9	7	4427.22645(20.)					
16	10	7	4665.97371(20.)					
17	0	17	2981.35920(20.)			4554.65190(30.)	4544.65299(50.)	4535.74571(40.)
17	1	17	2981.35920(20.)			4554.65190(30.)	4544.65299(50.)	4535.74571(40.)
17	1	16	3291.14905(15.)			4902.61401(5.)		
17	2	16	3291.15355(20.)			4902.62658(10.)		
17	2	15	3567.17320(30.)		3552.49481(400.)	5204.74861(25.)		
17	3	15	3567.25420(30.)			5204.98857(10.)		
17	3	14	3810.93659(8.)			5466.40269(8.)		
17	4	14	3812.04672(10.)			5469.18470(60.)		
17	4	13	4017.90825(7.)			5680.54750(50.)		
17	5	13	4027.50616(20.)			5700.48173(100.)		
17	5	12	4174.28733(20.)			5835.28649(100.)		
17	6	12	4221.03970(25.)			5911.62868(20.)		
17	6	11	4291.90670(30.)			5965.71452(35.)		
17	7	11	4409.34403(35.)					
17	7	10	4428.11400(40.)					
17	8	10	4610.02150(40.)					
17	8	9	4612.79063(15.)					
17	9	9	4830.61350(60.)					
17	9	8	4830.89460(40.)					
17	10	8	5070.00948(100.)					
17	10	7	5070.03158(50.)					
18	0	18	3319.44785(50.)			4889.48760(25.)		
18	1	18	3319.44785(50.)			4889.48760(25.)		
18	1	17	3647.46003(40.)			5258.61700(200.)		
18	2	17	3647.46113(40.)			5258.62316(100.)		
18	2	16	3940.54462(25.)			5579.35830(80.)		
18	3	16	3940.58703(30.)			5579.49150(30.)		
18	3	15	4201.25281(20.)			5859.61579(200.)		
18	4	15	4201.85865(20.)			5861.24000(150.)		
18	4	14	4427.16426(30.)			6095.51400(100.)		
18	5	14	4432.85969(40.)			6108.28000(150.)		
18	5	13	4606.16827(45.)					
18	6	13	4638.64463(20.)					
18	6	12	4735.84521(100.)					
18	7	12	4833.20812(20.)					
19	0	19	3675.11340(20.)			5241.74169(15.)		
19	1	19	3675.11340(20.)			5241.74169(15.)		
19	1	18	4021.21410(150.)			5632.04248(15.)		
19	2	18	4021.21460(100.)			5632.04788(50.)		
19	2	17	4331.06635(50.)			5970.92917(100.)		
19	3	17	4331.08904(50.)			5971.00428(200.)		
19	3	16	4608.22313(30.)					
19	4	16	4608.55740(40.)					
19	4	15	4851.82035(30.)					
19	5	15	4855.15165(40.)					
19	5	14	5052.66880(30.)					
20	0	20	4048.25225(200.)			5611.33160(100.)		
20	1	20	4048.25225(200.)			5611.33160(100.)		
20	1	19	4412.31235(200.)			6022.79300(250.)		

surements from this study and those of the (010)–(000) bands given in Ref. (*10*). The result of this analysis gives added levels for the ground state to those listed in the earlier work (*10*). These additional levels were for the higher *J* and K_a values.

C. Table 2

Table 2 lists values of the rotational energies obtained in this study for the (000) and (010) states along with associated, estimated uncertainties given within parentheses. The values are given with either six or five significant figures after the decimal, where those with six places were derived entirely from the analysis of microwave (*4*) and far-IR (*5*) measurements for the (000) state of $H_2{}^{16}O$ while those given with five significant figures past the decimal for the ground state of $H_2{}^{18}O$ were taken from Ref. (*10*).

5. LINESTRENGTHS

The strength, *S*, of an H_2O transition at frequency ν may be expressed to good approximation by

TABLE 3
Matrix Elements Used in the Expansion of the Dipole Moment for *B*-Type Transitions of Water Vapor

j	n	$\langle J\ K\vert A'(j)\vert J'K'\rangle / \langle J\ K\vert \Phi(x)\vert J'K+\Delta K\rangle$	$\Delta K = \pm 1$
2	1	$J'(J'+1) + J(J+1)$	
3	1	$K'^2 + K^2$	
4	1	$K'^2 - K^2$	
5	1	$K'^2 - K^2 - 2m$	
6	1	$(K'^2-K^2)(K'^2-K^2-2m)$	
7	1	$J(J+1) - 2m(m-1) + (2m-1)K\Delta K - K^2 -1$	
8	3	$[(J'-K\Delta K-1)(J'-K\Delta K-2)(J'+K\Delta K+2)(J'+K\Delta K+3)]^{1/2}$	
9	1	$K'^2J'(J'+1) - K^2J(J+1)$	
10	1	$K'^4 - K^4$	
11	1	$(K'^2-K^2)[J'(J'+1) + J(J+1)]$	
12	1	$K'^2(J'^2+J')^2$	
13	1	K'^6	
14	1	K'^4	
15	1	$K'^2J'(J'+1)$	
16	1	$K'^6 - K^6$	
17	1	$J'(J'+1)$ if $m=0$ and $J=K_c$ or $J'=K_c'$, otherwise $= 0$	
18	1	$J'(J'+1)$ if $m=0$ and $J=K_c$ or $J'=K_c'-1$, otherwise $= 0$	
19	1	$J'(J'+1)$ if $m\neq0$ and $J=K_c$ and $J'=K_c'$, otherwise $= 0$	

$J'-J = 0, \pm1$

$m = [J'(J'+1) - J(J+1)]/2$

$K'-K = n\Delta K$

$$S = C(\nu/Q)(g/T)[1 - \exp(-\nu/kT)] \times \exp(-E(L)/kT)|R(L, U)|^2,$$

where

$$C = 8\pi^3/3hc$$

$$Q = Q_V \times Q_R$$

and

$$E(L) = E_V(L) + E_R(L), \qquad [1]$$

where Q is the partition function which can be expressed as the product of the vibrational, Q_V, and rotational, Q_R, partition functions; g is the degeneracy caused by the nuclear spin of the lower state level; k is the Boltzmann constant; T is the temperature; $E(L)$ is the lower state energy equal to the sum of the lower state vibrational energy, $E_V(L)$, and rotational energy, $E_R(L)$; and $R(L, U)$ is the vibration–rotation dipole moment matrix element connecting the lower state, L, with the upper state, U. When $T = 296$ K, $Q_R = 174.6$ and $Q_V = 1.0004$ for $H_2{}^{16}O$ and for temperatures within 30° K of 300 K, $Q(T) = Q$ (296 K) $[296/T]^{3/2}$.

Without considering near resonance effects, the vibration–rotation dipole moment element, $R(L, U)$, given in Eq. [1], can be expressed as

$$R(L, U) = \sum_j u(j) \times (j)$$

$$x(j) = \langle J''K_a''K_c''|\langle V''|A(j)|V'\rangle|J'K_a'K_c'\rangle, \qquad [2]$$

where $u(j)$ are the dipole moment coefficients; $A(j)$ are the

TABLE 4
Dipole Moment Expansion Coefficients Derived from Least-Squares Fit of the (010)–(000), (000)–(000), and (010)–(010) Bands of $H_2{}^{16}O$

j	(010) - (000) band	(010) - (000) band	(010) - (000) band
1	$1.301(32)\times10^{-1}$	$1.295(32)\times10^{-1}$	$1.305(45)\times10^{-1}$
2	$5.48(191)\times10^{-5}$	$1.48(163)\times10^{-5}$	$7.46(634)\times10^{-6}$
3	$5.91(59)\times10^{-4}$	$5.31(372)\times10^{-5}$	$-2.24(11)\times10^{-4}$
4	$-5.72(57)\times10^{-3}$	$-6.98(70)\times10^{-3}$	$-6.32(32)\times10^{-3}$
5	$-1.86(242)\times10^{-4}$	$-3.01(150)\times10^{-4}$	$-1.44(108)\times10^{-4}$
6	$-4.83(242)\times10^{-5}$	$-3.61(126)\times10^{-5}$	$-1.70(76)\times10^{-5}$
7	$2.12(42)\times10^{-4}$	$5.78(202)\times10^{-5}$	$1.44(180)\times10^{-5}$
8	$-4.26(85)\times10^{-5}$	$-1.85(130)\times10^{-5}$	$-1.39(21)\times10^{-5}$
9	$-1.21(24)\times10^{-5}$	$-1.19(54)\times10^{-5}$	$-3.20(561)\times10^{-7}$
10	$6.74(34)\times10^{-5}$	$2.28(91)\times10^{-5}$	$1.87(10)\times10^{-5}$
11	$1.08(16)\times10^{-5}$	$4.27(192)\times10^{-6}$	$5.35(375)\times10^{-7}$
12	$-2.26(814)\times10^{-9}$	$1.00(640)\times10^{-9}$	$-3.68(166)\times10^{-9}$
13	$-1.15(40)\times10^{-7}$	$3.99(398)\times10^{-8}$	$6.14(430)\times10^{-9}$
14	$-5.34(240)\times10^{-6}$	$-4.20(189)\times10^{-6}$	$1.92(29)\times10^{-6}$
15	$2.04(112)\times10^{-6}$	$-8.75(744)\times10^{-6}$	$2.41(181)\times10^{-7}$
16	$-3.54(53)\times10^{-7}$	$-1.32(918)\times10^{-8}$	$-6.92(104)\times10^{-8}$
17	$9.7(150)\times10^{-5}$	$4.8(159)\times10^{-5}$	$-1.34(518)\times10^{-5}$
18	$1.9(155)\times10^{-5}$	$3.1(122))\times10^{-5}$	$-7.9(577)\times10^{-6}$
19	$5.59(727)\times10^{-5}$	$2.2(241)\times10^{-5}$	$1.0(126)\times10^{-5}$
N[b]	284	482	337
σ%[c]	2.57	2.62	3.45
min ν	$839.643 cm^{-1}$	$1403.462 cm^{-1}$	$1801.324 cm^{-1}$
max ν	$1399.204 cm^{-1}$	$1799.616 cm^{-1}$	$2568.790 cm^{-1}$

j	(000) - (000) band	(010) - (010) band
1	$1.778(95)\times10^{-0}$	$1.796(9)\times10^{-0}$
2	$-8.16(285)\times10^{-4}$	$1.87(9)\times10^{-4}$
3	$1.45(25)\times10^{-3}$	$1.13(6)\times10^{-3}$
4	$-5.7(241)\times10^{-4}$	$2.47(12)\times10^{-3}$
5	$-1.18(41)\times10^{-2}$	$-5.76(29)\times10^{-3}$
6	$2.92(146)\times10^{-4}$	$5.31(27)\times10^{-5}$
7	$-2.64(661)\times10^{-4}$	$-1.29(6)\times10^{-3}$
8	$-1.19(352)\times10^{-5}$	$-1.83(9)\times10^{-4}$
9	$3.30(99)\times10^{-5}$	
10	$1.16(98)\times10^{-5}$	$-7.96(40)\times10^{-6}$
11	$2.85(86)\times10^{-5}$	
12	$-8.7(117)\times10^{-9}$	
13	$9.44(377)\times10^{-8}$	
14	$-1.30(32)\times10^{-5}$	
15	$-6.26(250)\times10^{-6}$	$-1.62(8)\times10^{-5}$
16	$-2.41(72)\times10^{-7}$	
N[b]	226	24
σ%[c]	5.59	4.13
min ν	$590.331 cm^{-1}$	$601.592 cm^{-1}$
max ν	$1196.025 cm^{-1}$	$793.705 cm^{-1}$

Note. Values given in Debyes.

[a] Values given within parentheses are uncertainties in the last digit(s).

[b] N represents the number of line strengths used in the least-squares fits.

[c] σ% is the standard deviation resulting from the least-squares fit in percent; $\sigma\%\text{-}\{\Sigma[(S_{obs} - S_{cal})/S_{obs}]^2/N\}^{1/2} \times 100$.

transformed transition moment operators and prime and double prime denote upper and lower states, respectively. $x(1)$ is the matrix element of the direction cosines in which $A(1) = \Phi_\alpha$ with $\alpha = z$ for *A*-type transitions and $\alpha = x$ for *B*-type transitions. The asymmetric-top wavefunctions, $|JK_aK_c\rangle$, are expressed as an expansion of symmetry-adapted wavefunctions as discussed in Ref. (*1*).

The matrix elements involved in $R(L, U)$ were presented in Refs. (*1*) and (*10*) and also used here and are given in Table 3. The matrix elements, $x(j)$, were derived from the vibration–rotation frequency constants given in Ref. (*1*) for the (000) and (010) states of $H_2{}^{16}O$. The coefficients, $u(i)$, were determined from a least-squares fit of the experimental linestrengths using Eqs. [1] and [2] and the elements given in Table 3. Measured linestrengths were normalized to a temperature of 296 K by using Eq. [1] and lower state

TABLE 5
Line Positions (cm^{-1}) and Strengths (cm^{-2}/atm at 296 K) Observed in the (010)–(010) Band of $H_2{}^{16}O^a$

observed		upper			lower			lower	------------strength-------------			
position	(o-c)	J	K_a	K_c	J	K_a	K_c	energy	observed	%s	computed	(o-c)%
590.60010	-16.	8	4	4	7	1	7	2181.08986	1.70E-05	15.	2.37E-05	-39.4
601.59233	21.	8	5	3	7	2	6	2318.53988	2.34E-05	8.	2.41E-05	-3.0
602.13081	7.	12	3	9	11	2	10	3136.41252	1.05E-05	8.	1.04E-05	1.0
607.55591	67.	6	6	0	5	3	3	2126.40768	3.88E-06	5.	4.01E-06	-3.4
609.71606	4.	11	2	9	10	1	10	2705.13959	8.10E-05	8.	8.73E-05	-7.8
618.17328	30.	11	3	9	10	0	10	2705.09685	2.66E-05	32.	2.89E-05	-8.6
622.84006	-98.	7	6	2	6	3	3	2282.58956	7.66E-06	15.	7.16E-06	6.5
625.66409	22.	12	5	8	11	2	9	3314.85561	1.47E-05	6.	1.49E-05	-1.4
633.72130	5.	7	6	1	6	3	4	2271.71221	2.22E-05	6.	2.17E-05	2.3
635.11436	18.	12	4	9	11	1	10	3135.76472	2.45E-05	21.	2.86E-05	-16.7
638.24850	-6.	8	6	3	7	3	4	2462.87526	2.32E-05	5.	2.31E-05	.4
645.88043	27.	9	5	4	8	2	7	2495.16582	5.54E-05	24.	4.37E-05	21.1
650.14023	5.	9	6	4	8	3	5	2670.78960	5.11E-06	28.	6.24E-06	-22.1
660.03462	-3.	10	6	5	9	3	6	2904.67039	1.26E-05	4.	1.25E-05	.8
661.09963	12.	9	4	5	8	1	8	2337.66680	3.03E-05	10.	2.88E-05	5.0
661.18758	-16.	8	6	2	7	3	5	2439.95442	6.66E-06	16.	7.63E-06	-14.6
664.78212	37.	13	5	9	12	2	10	3587.66670	1.64E-06	15.	1.63E-06	.6
666.43141	-3.	13	3	10	12	2	11	3386.37950	9.97E-06	8.	9.38E-06	5.9
671.77240	0.	12	2	10	11	1	11	2915.89430	1.10E-05	13.	1.09E-05	.9
676.54954	-5.	12	3	10	11	0	11	2915.87433	3.30E-05	12.	3.25E-05	1.5
682.24561	-15.	12	6	7	11	3	8	3441.03957	1.75E-06	15.	3.46E-06	-97.7
687.98590	-44.	13	4	10	12	1	11	3386.05234	3.09E-06	7.	2.99E-06	3.2
690.82072	-5.	9	6	3	8	3	6	2630.19257	1.77E-05	4.	1.72E-05	2.8
696.80661	-48.	10	5	5	9	2	8	2690.59359	8.60E-06	20.	6.67E-06	22.4
708.26008	-70.	14	5	10	13	2	11	3877.08862	1.39E-06	15.	1.36E-06	2.2
711.52929	-86.	7	7	0	6	4	3	2398.38146	4.15E-06	15.	3.02E-06	27.2
721.23373	62.	14	6	9	13	3	10	4052.81094	6.18E-07	15.	4.57E-07	26.1
723.57274	-7.	10	6	4	9	3	7	2841.43075	3.01E-06	8.	3.30E-06	-9.6
732.50967	-18.	13	2	11	12	1	12	3144.57877	1.10E-05	7.	1.11E-05	-.9
734.15616	15.	8	7	2	7	4	3	2572.13915	4.37E-06	5.	4.45E-06	-1.8
735.15150	9.	13	3	11	12	0	12	3144.56930	3.60E-06	15.	3.70E-06	-2.8
736.78743	-15.	8	7	1	7	4	4	2569.50794	1.50E-06	5.	1.50E-06	.0
741.36215	-20.	10	4	6	9	1	9	2512.37563	2.96E-06	15.	2.97E-06	-.3
742.00255	-6.	14	4	11	13	1	12	3654.04886	2.51E-06	12.	2.53E-06	-.8
755.47550	-20.	11	5	6	10	2	9	2904.42833	7.50E-06	6.	6.97E-06	7.1
760.41818	11.	11	6	5	10	3	8	3072.72635	4.47E-06	11.	4.51E-06	-.9
761.93012	9.	9	7	2	8	4	5	2764.69742	4.22E-06	13.	3.96E-06	6.2
771.94530	25.	10	7	4	9	4	5	2998.76631	2.40E-06	8.	2.52E-06	-5.0
784.61337	-21.	11	7	5	10	4	6	3253.73798	5.78E-07	15.	4.35E-07	24.7
787.40148	-1.	10	7	3	9	4	6	2983.32302	9.87E-07	15.	8.52E-07	13.7
788.38923	-6.	15	3	12	14	2	13	3939.83187	6.23E-07	15.	6.50E-07	-4.3
792.25824	-11.	14	2	12	13	1	13	3391.13066	1.23E-06	15.	1.15E-06	6.5
793.70515	8.	14	3	12	13	0	13	3391.12616	3.24E-06	1.	3.42E-06	-5.6
802.32924	-5.	12	6	6	11	3	9	3323.26983	6.97E-07	15.	5.43E-07	22.1
822.84008	-87.	12	5	7	11	2	10	3136.41252	4.72E-07	15.	6.22E-07	-31.8
830.73081	-10.	11	4	7	10	1	10	2705.13959	2.50E-06	15.	2.25E-06	10.0
832.78261	-69.	9	8	1	8	5	4	2919.63292	8.43E-07	15.	6.66E-07	21.0
850.28955	29.	13	6	7	12	3	10	3592.42392	6.67E-07	15.	4.65E-07	30.3
851.24876	4.	15	2	13	14	1	14	3655.48514	7.82E-07	15.	9.67E-07	-23.7

energies given in Table 2. A fitting scheme used in Refs. (*1*) and (*10*) was also used in the present work for the analysis of the measured linestrengths of the (010)–(000) band of $H_2{}^{16}O$ in which the measurements were separated into sets, with each set representing a frequency interval.

The analysis of the (010)–(000) band of $H_2{}^{18}O$ included over 100 lines measured in this study with strengths >0.5 cm^{-2}/atm (normalized to 100% of species) plus the measurements given in the earlier study (*10*) for the weaker transitions. The results for the (010)–(000) bands of $H_2{}^{16}O$ and $H_2{}^{18}O$ are similar to those given in Refs. (*1*) and (*10*), especially for the leading dipole term, *u*(1), which is directly related to values of the strongest linestrengths of a band. Therefore, it appears conclusive that the linestrength values of the strongest transitions given in the prior studies (*1*, *10*) are accurate. The linestrengths of the (010)–(000) band of $H_2{}^{17}O$ were not analyzed in this study; however, the results given in Ref. (*10*) should be accurate.

The dipole moment matrix elements, *u*(*i*), obtained from the

TABLE 6
Line Positions (cm^{-1}) and Strengths (cm^{-2}/atm at 296 K) Observed in the (000)–(000) Band of $H_2{}^{18}O$[a]

observed		upper			lower			lower	------------strength------------			
position	(o-c)	J	K_a	K_c	J	K_a	K_c	energy	observed	%s	computed	(o-c)%
595.52928	-17.	11	6	6	10	3	7	1534.36837	2.40E-05	15.	1.71E-05	28.8
598.02230	2.	12	4	9	11	1	10	1518.54258	1.15E-04	7.	1.20E-04	-4.4
606.14407	0.	7	5	3	6	0	6	444.84623	1.10E-05	9.	1.04E-05	5.9
612.52280	-5.	12	6	7	11	3	8	1808.36235	2.80E-05	9.	2.55E-05	9.0
614.20030	-12.	9	4	5	8	1	8	740.99874	8.83E-05	5.	8.72E-05	1.2
617.34993	-8.	9	6	3	8	3	6	1001.70586	1.02E-04	3.	1.01E-04	1.1
617.41000	0.	15	5	10	14	4	11	2735.41921	1.50E-06	15.	1.37E-06	8.4
623.29360	0.	13	5	9	12	2	10	1952.67815	6.71E-06	15.	8.56E-06	-27.6
627.95330	-12.	7	7	0	6	4	3	751.03301	1.85E-05	5.	1.85E-05	.2
631.21760	-3.	12	2	10	11	1	11	1321.46052	3.90E-05	4.	3.81E-05	2.3
633.19925	3.	12	3	10	11	0	11	1321.45434	1.20E-04	8.	1.14E-04	4.7
634.29320	0.	14	4	10	13	3	11	2239.02987	3.50E-06	15.	2.63E-06	24.9
634.83300	-62.	6	6	1	5	1	4	398.36052	2.80E-06	15.	1.82E-06	34.9
635.33342	0.	13	6	8	12	3	9	2099.56255	3.10E-06	15.	3.40E-06	-9.8
639.43125	1.	13	3	10	12	2	11	1767.33865	3.85E-05	4.	3.87E-05	-.6
640.29000	0.	10	5	5	9	2	8	1075.90952	3.05E-05	7.	2.85E-05	6.5
648.97825	8.	8	7	2	7	4	3	925.69983	3.05E-05	5.	2.93E-05	3.8
649.55750	-19.	13	4	10	12	1	11	1767.22511	1.47E-05	6.	1.28E-05	13.2
651.83400	-4.	10	6	4	9	3	7	1211.18576	2.00E-05	8.	1.98E-05	1.2
652.78260	5.	8	7	1	7	4	4	921.89590	9.30E-06	7.	9.99E-06	-7.4
662.59064	-11.	8	5	4	7	0	7	583.77780	2.60E-05	3.	2.59E-05	.5
668.81700	0.	14	5	10	13	2	11	2238.03200	6.50E-06	15.	7.19E-06	-10.7
677.74426	4.	9	7	2	8	4	5	1116.63623	3.37E-05	2.	2.81E-05	16.5
682.73470	-9.	10	7	4	9	4	5	1355.19916	2.01E-05	6.	1.91E-05	5.1
686.82692	-12.	13	2	11	12	1	12	1551.20496	3.97E-05	4.	3.93E-05	.9
687.82780	5.	13	3	11	12	0	12	1551.20212	1.35E-05	10.	1.31E-05	2.8
695.35990	-7.	10	4	6	9	1	9	916.29360	8.40E-06	6.	8.54E-06	-1.7
695.95060	2.	14	3	11	13	2	12	2033.81822	4.10E-06	10.	3.71E-06	9.5
697.73368	-5.	8	6	3	7	1	6	701.69433	1.31E-05	6.	1.24E-05	5.7
701.65351	0.	14	4	11	13	1	12	2033.76570	1.10E-05	3.	1.11E-05	-.6
701.77942	0.	12	7	6	11	4	7	1894.19577	5.60E-06	8.	5.09E-06	9.0
702.58920	-25.	11	5	6	10	2	9	1288.26735	2.75E-05	3.	2.87E-05	-4.5
703.48250	-15.	10	7	3	9	4	6	1334.47935	6.75E-06	4.	6.48E-06	4.0
709.60170	0.	13	7	7	12	4	8	2200.43888	1.00E-06	15.	7.13E-07	28.7
717.59820	-2.	8	8	1	7	5	2	1051.20326	4.10E-06	7.	4.22E-06	-2.9
717.81120	2.	8	8	0	7	5	3	1050.99030	1.36E-06	10.	1.39E-06	-2.3
719.35817	0.	14	7	8	13	4	9	2527.68887	5.00E-07	15.	7.89E-07	-57.7
725.10596	-6.	9	5	5	8	0	8	740.91235	4.95E-06	6.	5.09E-06	-2.9
730.85660	-3.	11	7	4	10	4	7	1574.44957	1.06E-05	2.	1.05E-05	.6
736.83725	-1.	12	6	6	11	3	9	1688.28644	3.70E-06	6.	3.32E-06	10.2
739.40135	-12.	9	6	4	8	1	7	879.49487	3.95E-06	8.	3.95E-06	-.1
741.70475	-3.	14	2	12	13	1	13	1798.96637	4.16E-06	7.	4.14E-06	.5
742.14589	10.	9	8	2	8	5	3	1247.20616	1.80E-06	12.	1.94E-06	-7.6
742.20725	8.	14	3	12	13	0	13	1798.96549	1.20E-05	4.	1.24E-05	-3.4
742.98335	-5.	9	8	1	8	5	4	1246.36855	6.00E-06	8.	5.85E-06	2.5
750.68353	0.	15	3	12	14	2	13	2318.13865	2.70E-06	5.	2.93E-06	-8.7
753.81320	0.	15	4	12	14	1	13	2318.11367	1.00E-06	25.	9.74E-07	2.6
760.85150	0.	12	7	5	11	4	8	1835.48680	1.60E-06	8.	1.54E-06	3.7
764.99025	-19.	10	8	3	9	5	4	1468.61221	4.95E-06	4.	4.75E-06	4.1
767.58460	-18.	10	8	2	9	5	5	1466.01837	2.07E-06	5.	1.59E-06	23.1
774.22232	11.	12	5	7	11	2	10	1518.78799	1.77E-06	15.	2.47E-06	-39.3
784.39360	-6.	11	4	7	10	1	10	1109.80211	6.10E-06	5.	6.64E-06	-8.9
787.69180	0.	10	6	5	9	1	8	1074.76308	7.65E-06	10.	7.81E-06	-2.0
789.69200	0.	13	6	7	12	3	10	1954.65356	2.20E-06	15.	2.87E-06	-30.6
793.28197	0.	10	5	6	9	0	9	916.25779	7.00E-06	5.	7.23E-06	-3.4
794.22487	-27.	8	7	2	7	2	5	780.45286	1.11E-06	15.	8.13E-07	26.7
794.49860	0.	13	7	6	12	4	9	2116.56486	1.80E-06	15.	1.66E-06	7.7
795.98380	0.	15	2	13	14	1	14	2064.67291	3.80E-06	8.	3.59E-06	5.6
796.23625	0.	15	3	13	14	0	14	2064.67225	1.20E-06	15.	1.20E-06	.1
800.97754	25.	9	9	0	8	6	3	1399.42806	7.78E-07	15.	7.52E-07	3.3

TABLE 6—*Continued*

observed		upper			lower			lower	------------strength------------			
position	(o-c)	J	K_a	K_c	J	K_a	K_c	energy	observed	%s	computed	(o-c)%
805.71546	0.	16	4	13	15	1	14	2620.17300	7.00E-07	15.	7.03E-07	-.4
814.15171	-66.	9	7	3	8	2	6	980.22238	4.88E-07	15.	5.09E-07	-4.4
816.05900	0.	12	8	4	11	5	7	1976.29723	6.40E-07	15.	4.54E-07	29.0
826.89835	-28.	10	9	2	9	6	3	1619.05587	9.00E-07	10.	9.03E-07	-.3
839.73440	11.	10	7	4	9	2	7	1198.19966	1.80E-06	6.	1.77E-06	1.8
841.00690	0.	13	8	5	12	5	8	2265.43837	6.30E-07	15.	5.38E-07	14.6
842.16338	41.	11	6	6	10	1	9	1287.73485	1.20E-06	7.	1.27E-06	-6.0
849.72920	0.	16	2	14	15	1	15	2348.24680	3.90E-07	15.	3.16E-07	19.0
849.83300	0.	16	3	14	15	0	15	2348.24680	1.80E-06	20.	9.50E-07	47.2
854.67062	0.	13	5	8	12	2	11	1767.33865	1.50E-06	10.	1.59E-06	-6.2
866.51041	26.	11	5	7	10	0	10	1109.78708	8.17E-07	15.	9.27E-07	-13.5
878.05708	-5.	9	6	3	8	1	8	740.99874	9.33E-07	15.	7.72E-07	17.2
878.97836	0.	12	4	8	11	1	11	1321.46052	5.25E-07	15.	5.32E-07	-1.3
902.34285	23.	12	6	7	11	1	10	1518.54258	1.35E-06	12.	1.45E-06	-7.6
943.98393	-10.	12	5	8	11	0	11	1321.45434	8.92E-07	15.	9.33E-07	-4.6

a. (o-c), observed minus computed line positions in $cm^{-1} \times 10^5$. The computed values and the lower state energies are derived from the energy level values given in Table 2. %s's are estimated uncertainties in the measured line strengths given in percent. (o-c)%, observed minus computed line strength values given in percent. Computed values are derived from constants obtained in this work and given in table 4.

individual least-squares fits of $H_2{}^{16}O$ are given in Table 4. Included in the listing are the number, N, of experimental values included in the fit, the standard deviation, $\sigma\%$, in percent, and the spectral range of lines used in each analysis. $\sigma\%$ is defined as

$$\sigma\% = \{\sum_n [(S_{\text{obs}} - S_{\text{cal}})/S_{\text{obs}}]^2/N\}^{1/2} \times 100. \qquad [3]$$

The values given in parenthesis in Table 4 are the uncertainties in the coefficients and these were determined by varying the value of each parameter while holding the others constant. The uncertainty of the parameter was established when the standard deviation of the computed strengths, σ', was equal to twice the standard deviation of the least-squares fit, 2σ.

Inspection of the table shows that the results for the (010)–(000) bands are given in terms of sets with each set representing a frequency interval. The same was also found in my earlier work (*1*) in which the theory in the present state is not adequate to take care of all the necessary measurements in one fitting procedure. Inspection of Table 4 shows a few terms of the (010)–(000) and (000)–(000) band with uncertainties much larger in magnitude than the values. For practical purposes, the values for these terms can be set to zero; however, they were included to indicate their magnitude and sign.

It was not necessary to separate the data into frequency intervals for fitting the pure rotational bands because the range of linestrength values were within the range (all strength values within about three to four orders of magnitude of each other) for the theory to operate sufficiently well with all measurements included in one fitting procedure.

The results from the $H_2{}^{18}O$ analysis of the (010)–(000) band measurements are not given in Table 4 because they prove no improvement over prior values given in Ref. (*10*). Also the linestrength measurements of the (000)–(000) bands of $H_2{}^{17}O$ and $H_2{}^{18}O$ were not analyzed; however, they can be computed to adequate accuracy using the dipole moment parameters of the (000)–(000) band of $H_2{}^{16}O$ which are given in Table 4.

6. RESULTS

The listing for the (010)–(000) and (000)–(000) bands of $H_2{}^{16}O$ are not given in this report. However, they will be presented in a following paper discussing linewidth measurements (*13*). The results for the (010)–(010) band are given here and listed in Table 5. The table lists the observed frequency, the difference between the observed and computed frequencies, (o–c), the rotational quantum assignment, lower state energy level, observed strength, estimated uncertainty in the measured strength in percent, %s, computed strength, and the percent difference between the observed and computed strength, (o–c)%. Measured strength values with %s = 15% represent uncertainties ranging between 50% and possibly less than 10% for one or more of the following reasons: (a) blending, (b) weakness of the transition, and (c) only one measurement was obtained for that line. Values with %s > 15% were the result of poor agreement between the linestrength values derived from the various spectra. Linestrength values included in the least-squares fits were those for which %$s \leq 8\%$ for the (010)–(000) band and %$s \leq 10\%$ for the (000)–(000) band and %$s \leq 14\%$ for the (010)–(010) band. The computed strengths were derived from Eq. [1] with the dipole moment parameters given in Table 4 and energy levels given in Table 2. The

TABLE 7
Line Positions (cm^{-1}) and Strengths (cm^{-2}/atm at 296 K) Observed in the (000)–(000) Band of $H_2{}^{17}O$[a]

observed		upper			lower			lower	------------strength	-------------		
position	(o-c)	J	K_a	K_c	J	K_a	K_c	energy	observed	%s	computed	(o-c)%
598.99870	13.	12	4	9	11	1	10	1521.51755	2.20E-05	5.	2.17E-05	1.3
609.33400	-89.	7	5	3	6	0	6	445.71922	1.90E-06	20.	1.90E-06	.1
615.06460	-40.	9	4	5	8	1	8	742.49085	1.80E-05	25.	1.59E-05	11.9
616.28037	0.	12	6	7	11	3	8	1810.66703	5.05E-06	15.	4.63E-06	8.4
621.06070	-30.	9	6	3	8	3	6	1003.78133	1.80E-05	6.	1.84E-05	-2.2
624.70300	220.	13	5	9	12	2	10	1956.23540	1.50E-06	15.	1.54E-06	-2.9
632.10680	-30.	12	2	10	11	1	11	1324.12830	6.50E-06	5.	6.90E-06	-6.2
632.71600	212.	7	7	0	6	4	3	753.70510	2.50E-06	25.	3.37E-06	-34.7
634.23646	-12.	12	3	10	11	0	11	1324.12157	2.25E-05	8.	2.07E-05	8.0
638.55100	275.	13	6	8	12	3	9	2102.55395	6.00E-07	15.	6.15E-07	-2.6
639.70390	-210.	13	3	10	12	2	11	1770.83503	5.24E-06	15.	6.94E-06	-32.4
655.29581	-70.	10	6	4	9	3	7	1213.56231	3.40E-06	10.	3.60E-06	-5.9
665.55720	-60.	8	5	4	7	0	7	584.94089	6.18E-06	10.	4.74E-06	23.3
694.37868	-6.	11	6	5	10	3	8	1443.04107	5.00E-06	5.	4.96E-06	.8
696.49000	188.	14	3	11	13	2	12	2037.85408	6.50E-07	15.	6.64E-07	-2.1
702.26205	-9.	8	6	3	7	1	6	702.88597	2.37E-06	10.	2.26E-06	4.5
703.86487	-46.	11	5	6	10	2	9	1290.79853	4.80E-06	8.	5.18E-06	-8.0
723.05162	-87.	8	8	1	7	5	2	1055.25530	7.07E-07	15.	7.65E-07	-8.2
727.82697	0.	9	5	5	8	0	8	742.39857	1.16E-06	15.	9.29E-07	19.9
735.40950	-3.	11	7	4	10	4	7	1577.68835	2.06E-06	4.	1.91E-06	7.1
739.43947	0.	12	6	6	11	3	9	1691.48503	4.39E-07	15.	6.04E-07	-37.6
742.89095	0.	14	2	12	13	1	13	1802.60001	1.00E-06	15.	7.46E-07	25.4
743.43840	0.	14	3	12	13	0	13	1802.59895	2.08E-06	4.	2.24E-06	-7.6
743.59451	0.	9	6	4	8	1	7	881.09903	7.91E-07	15.	7.20E-07	9.0
748.45766	0.	9	8	1	8	5	4	1250.49869	8.43E-07	15.	1.06E-06	-25.2
770.62900	24.	10	8	3	9	5	4	1472.68499	1.00E-06	5.	8.62E-07	13.8
774.81526	0.	12	5	7	11	2	10	1521.78224	3.00E-07	15.	4.44E-07	-48.0
784.41420	15.	11	4	7	10	1	10	1112.04116	1.15E-06	15.	1.20E-06	-4.8
791.53015	41.	10	6	5	9	1	8	1076.80099	1.40E-06	10.	1.42E-06	-1.8
795.74755	0.	10	5	6	9	0	9	918.10200	7.01E-07	15.	1.32E-06	-87.8
797.31562	-91.	11	8	3	10	5	6	1713.84955	4.89E-07	15.	5.15E-07	-5.3

a. (o-c), observed minus computed line positions in $cm^{-1} \times 10^5$. The computed values and the lower state energies are derived from the energy level values given in Table 2. %s's are estimated uncertainties in the measured line strengths given in percent. (o-c)%, observed minus computed line strength values given in percent. Computed values are derived from constants obtained in this work and given in table 4.

computed line positions were determined from the levels given in Table 2.

It was stated earlier in this report that the linestrengths of the (000)–(000) bands of $H_2{}^{18}O$ and $H_2{}^{17}O$ could be adequately computed from the $H_2{}^{16}O$ dipole moment parameters of this band. This is displayed in Table 6 for $H_2{}^{18}O$ and Table 7 for $H_2{}^{17}O$. These tables are given in the same format as that of Table 5. The computed frequencies were derived from the energy level values given in Table 2 and the computed strengths were calculated using Eq. [2] and, as noted, the parameters for the (000)–(000) band of $H_2{}^{16}O$ given in Table 4.

7. DISCUSSION AND CONCLUSIONS

The line positions of over 1700 lines of H_2O were measured at high spectral resolution and low sample pressures with the samples near or at room temperature with absorption path lengths up to 433 m. The transition frequencies were determined to an absolute accuracy of 0.0001 cm^{-1} (3 MHz) or better for the majority of the lines with an uncertainty in the precision of the measurements of 6×10^{-5} cm^{-1}. These data were used in conjunction with microwave (*4*), far-IR (*5*), and hot water emission spectra (*6–10*) along with previous measurements reported by this author (*1, 10*) to determine accurate values for energy levels for the (000) and (010) vibrational states of $H_2{}^{16}O$, $H_2{}^{17}O$, and $H_2{}^{18}O$. The methods used to determine the ground and higher state energy level values are the same as that discussed and applied in Ref. (*1*). The analysis was limited to transitions that are or may be observed in earth atmospheric experiments.

Three other studies of high-resolution $H_2{}^{16}O$ absorption frequency measurements involving the (000)–(000) or (010)–(000) bands were reported by Guelachvili (*18*), Johns (*19*), and

Paso and Horneman (*20*). These data were not included in the present analysis because the majority of the measurements (*18–20*) were of the stronger transitions of which the levels involved were well covered in the measurements from the present study as well as the very high accuracy measurements from microwave (*4*) and far-IR (*5*) studies which were included in the analysis. Also the weaker transitions involving higher J and/or K_a levels reported in Refs. (*18–20*) were also well covered in the data used in this study with an overall higher precision due to the high optical paths applied here which were at least 10 times larger than used in any of the earlier studies.

The experimental linestrengths were fitted by least squares to a theoretical model developed and used earlier (*1*, *10*). The model included 19 matrix elements with several terms empirically derived. The model is not perfect, which is reflected by the necessity to separate the data of the (010)–(000) band of $H_2{}^{16}O$ into three sets. However, it was not necessary to separate the data into frequency intervals for fitting the pure rotational bands because the range of linestrength values were within the range (all strength values within about three to four orders of magnitude of each other) for the theory to operate sufficiently well with all measurements included in one fitting procedure.

8. ACKNOWLEDGMENTS

The author thanks the Kitt Peak National Observatory for the use of the FTS and C. Plymate for assistance in obtaining the H_2O spectra. The author also thanks L. Brown for making the short path length, foreign-broadening spectra available to him for this study. The research described in this paper was performed at the Jet Propulsion Laboratory, California Institute of Technology, under contract with The National Aeronautics and Space Administration.

REFERENCES

1. R. A. Toth, *J. Opt. Soc. Am. B* **8,** 2236–2255 (1991).
2. R. A. Toth, *J. Opt. Soc. Am. B* **10,** 1526–1544 (1993).
3. R. A. Toth, *J. Opt. Soc. Am.* **10,** 2006–2029 (1993).
4. J. C. Pearson, T. Anderson, E. Herbst, F. C. De Lucia, and P. Helminger, *Astrophys. J.* **379,** L41–L43 (1991).
5. F. Matsushima, H. Odashima, T. Iwasaki, S. Tsunekawa, and K. Takagi, *J. Mol. Struct.* **352 353,** 371–378 (1995).
6. O. L. Polyansky, J. R. Busler, B. Guo, K. Zhang, and P. Bernath, *J. Mol. Spectrosc.* **176,** 305–315 (1996).
7. S. Viti, J. Tennyson, and O. L. Polyansky, *Mon. Not. R. Astron. Soc.* **287,** 79–86 (1997).
8. O. L. Polyansky, N. F. Zobov, S. Viti, J. Tennyson, P. F. Bernath, and L. Wallace, *Science* **277,** 346–348 (1997).
9. O. L. Polyansky, N. F. Zobov, S. Viti, J. Tennyson, P. F. Bernath, and L. Wallace, *J. Mol. Spectrosc.,* in press.
10. R. A. Toth, *J. Opt. Soc. Am. B* **9,** 462–482 (1992).
11. L. H. Coudert, *J. Mol. Spectrosc.* **181,** 246–273 (1997).
12. R. A. Toth, L. R. Brown, and C. Plymate, ‘‘Self-broadened widths and frequency shifts of water vapor from 590 cm^{-1} to 2400 cm^{-1},’’ *J. Quant. Spectrosc. Radiat. Transfer* **59,** (1998), 529–562.
13. R. A. Toth, *J. Quant. Spectrosc. Radiat. Transfer*, in press.
14. L. R. Brown, R. A. Toth, and C. Plymate, *J. Quant. Spectrosc. Radiat. Transfer*, in preparation.
15. R. A. Toth, *Appl. Opt.* **30,** 5289–5315 (1991).
16. L. S. Rothman, R. R. Gamache, A. Goldman, L. R. Brown, R. A. Toth, H. Pickett, R. Poynter, J.-M. Flaud, C. Camy-Peyret, A. Barbe, N. Husson, C. P. Rinsland, and M. A. H. Smith, *Appl. Opt.* **26,** 4058–4097 (1987).
17. J. K. G. Watson, *J. Chem. Phys.* **46,** 1935–1949 (1967).
18. G. Guelachvili, *Opt. Soc. Am.* **73,** 137–150 (1983).
19. J. W. C. Johns, *J. Opt. Soc. Am. B* **2,** 1340–1354 (1985).
20. R. Paso and V.-M. Horneman, *J. Opt. Soc. Am. B* **12,** 1813–1838 (1995).